University Library

MINERVA ACCESS

A gateway to Melbourne's research publications

Minerva Access is the Institutional Repository of The University of Melbourne

Author/s:
Ren, J;Zhang, L;Walkley, B;Black, JR;San Nicolas, R

Title:
Degradation resistance of different cementitious materials to phosphoric acid attack at early stage

Date:
2022-01-01

Citation:
Ren, J., Zhang, L., Walkley, B., Black, J. R. & San Nicolas, R. (2022). Degradation resistance of different cementitious materials to phosphoric acid attack at early stage. Cement and Concrete Research, 151, https://doi.org/10.1016/j.cemconres.2021.106606.

Persistent Link:
https://hdl.handle.net/11343/292043

Degradation resistance of different cementitious materials to phosphoric acid attack at early stage

Jie Ren[1, 2], Lihai Zhang[1], Brant Walkley[3], Jay R. Black[4], Rackel San Nicolas[1 *]

[1] Department of Infrastructure Engineering, the University of Melbourne, Victoria, 3010, Australia

[2] Guangdong Provincial Key Laboratory of Durability for Marine Civil Engineering, College of Civil and Transportation Engineering, Shenzhen University, Shenzhen 518060, China

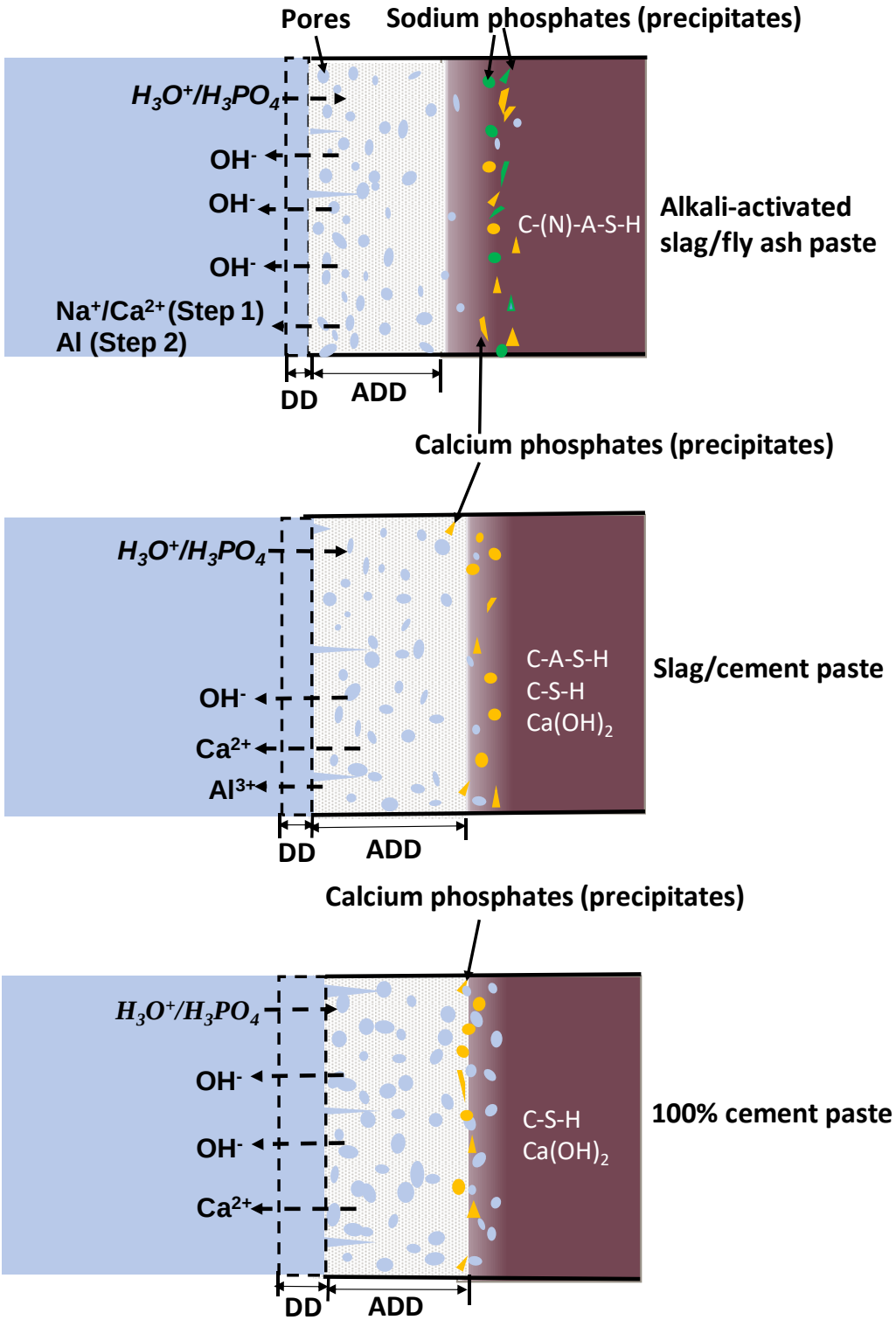
[3]Department of Chemical and Biological Engineering, The University of Sheffield, Sheffield S1 3JD, UK

[4] School of Earth Sciences, Peter Cook Centre for CCS Research, The University of Melbourne, VIC 3010 Australia

Abstract

Sewer wastewater systems pose great threats to OPC-based concretes used for pipes due to the presence of various acids. Phosphoric acid can cause as much damage as sulphuric acid but has been very lightly studied. This study focuses on the early stage of the degradation process of different cementitious materials in phosphoric acid. Three types of cementitious materials are compared: OPC (100% cement), slag-blended OPC (slag/cement mass ratio at 65/35) and alkali-activated slag/fly ash pastes (slag/fly ash mass ratio at 50/50). Samples were exposed to phosphoric acid solution with a constant pH at 2.0 ± 0.2 for 44 days. The degradation kinetics, chemical and microstructural properties as well as dissolution rate of these binders are analysed. The results show that the alkali-activated slag/fly ash binder has the lowest degradation rate compared to the other cement-based binders. The intrinsic characteristics of the binders lead to significant changes in the kinetics of degradation. The chemical properties of the binders are the critical influential factor of the early stage behaviour. A conceptual degradation process is proposed to describe the early-stage kinetics of degradation for the cementitious materials studied.

Keywords: Phosphoric acid; Early stage; Alkali-activated slag/fly ash binders; Degradation resistance



Graphical abstract

Schematic diagram showing the early stage degradation processes of AASF and OPC-based pastes exposed to the phosphoric acid. ADD-Apparent degradation depth; DD-Dissolved/detached depth.

1. Introduction

The resistance of cementitious materials exposed to acidic environments, such as sewage wastewater pipes containing effluents, has seen a recent growth in academic and industrial interest [1-14] due to immense costs of maintaining this infrastructure. When exposed to acidic agro-industrial wastewaters, cementitious materials suffer from severe deterioration due to reactions between their alkaline matrix and various acids [15-19].

Phosphates ($H_2PO_4^-$, HPO_4^{2-} or PO_4^{3-}), are one of the main components in silage effluent discharged by agricultural practices with a resultant acidic condition (pH ≈ 3.5-5) [20], posing severe challenges for cementitious materials used in sewer networks [8, 21, 22]. According to related research [23], fertilizer production could produce a dilute mixture of phosphoric, sulfuric and even fluosilic acids with pH level as low as 1 to 2. Previous studies have shown that the exposure of OPC concretes to phosphoric acid (pH = 2, 3 or 4) or phosphate-rich acidic environments resulted in significant degradation [1, 8, 24].

It has been reported that the degradation process of cementitious binders caused by acid attacks is a synergistic effect of chemical reactions which generally dominate early stage degradation and physical ion diffusion which is more obvious during later stages [25, 26]. Specially, chemical reactions occur at the surface of cementitious binders first, forming different chemical products and a degraded layer. With the thickness of the degraded layer gradually increasing, the acid solution has to diffuse the degraded layer before reaching undegraded components and triggering new reactions. It is apparent the early stage degradation process is critical for the entire performance of cementitious binders as it determines the reaction products, i.e. different types of calcium salts, and formation of degraded layer which could significantly influence the subsequent degradation evolutions [16, 27, 28]. Despite recent advances, there remains a lack of understanding of the degradation effect and related mechanisms of phosphoric acid on cementitious materials, particularly during early stages.

Alkali-activated materials (AAMs) are a viable alternative with potential to replace OPC-based binders due to their lower CO_2 footprint, comparable mechanical strength and enhanced durability, especially acid resistance compared to their OPC counterparts. Among all types of AAMs, alkali-activated slag/fly ash (AASF) has become more appealing due to some disadvantages and limitations when only fly ash (FA) or slag is used [29-32]. Specifically, the use of FA as the only precursor often requires heat curing to achieve structural integrity at early ages [33], which is not practical for in-situ industrial applications. For alkali-activated slag, the main reaction product after hydration reaction is an aluminium-substituted calcium silicate

hydrate gel (C-(A)-S-H gel) with a low Ca/Si ratio [34]. This type of gel is reported to be more susceptible towards acidic degradation due to its higher calcium content as compared to the sodium aluminosilicate hydrate (N-A-S-H) type gels in FA-based AAMs [35, 36]. In comparison, AASF binders contain both C-(A)-S-H and N-A-S-H gels [37-39] which are expected to mitigate the abovementioned problems that single slag or FA-based AAMs have.

Durability of AASF binders in acid environments has been partially investigated in some literature and it is confirmed that although AASF binders generally have a certain resistance capacity towards some acid attacks such as sulphuric and nitric, they may still suffer from severe deteriorations such as the formation of a degraded product layer along with corroded depth. "Corroded depth" is here defined as in some literature as an area with lower pH and other possible change in the nature of the binder [40-42]. However, related research focusing on their behaviour under phosphoric acid attack and detailed comparisons with OPC-based binders is far from adequate [8].

This study aims to investigate the early stage degradation of AASF (slag/FA = 1 by mass) in phosphoric acid solutions and another two types of OPC-based binders are used as references. The blended OPC binder usage is based on studies [19, 43] which reported that supplementary cementitious materials rich in Al (such as slag in this study) could improve the acid resistance by improving the microstructure and integrity of degraded layers. Various indicators including degradation depth, mass changes and leaching rates of ions were employed in the study to monitor the degradation kinetics. Chemical and microstructural analysis were also used to characterise their resistance to degradation by phosphoric acid at early stages. Finally, conceptual descriptions of the degradation for all binders are proposed.

2. Materials and methods

2.1. Materials

A type of FA (class F) according to ASTM C618 and grand granulated blast furnace slag (GGBFS) were used as precursors for AASF binders, supplied by CEMENT AUSTRALIA and Independent Cement and Lime Pty. Ltd., respectively. The FA and GGBFS has a specific gravity of 2,800 and 2,200 kg/m^3 respectively and their corresponding median particle size (d_{50}) was 14 for FA and 25 μm for GGBFS. A GP (General purpose) type OPC (Eureka Cement, Australia) in accordance with AS 3972 with a specific gravity between 2,800-3,200 kg/m^3 and bulk density 1,200-1,600 kg/m^3 was used. Their chemical compositions and X-ray diffraction (XRD) patterns are shown in Table 1 and Fig. 1 (FA an GGBFS) and Fig. 2 (OPC), respectively. According to Fig. 1, FA contains some crystalline phases such as mullite, quartz and hematite.

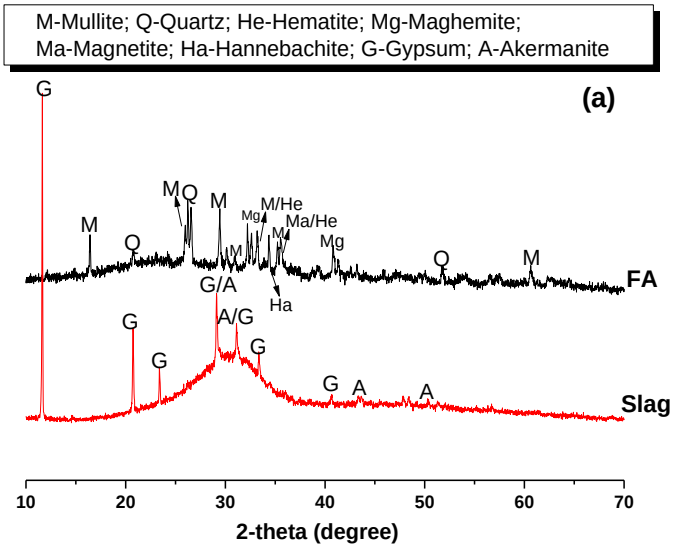
In comparison, GGBFS was mainly amorphous evidenced by a broad diffuse hump between 25 and 35 ° (2θ) with a few Akermanite and gypsum. Generally, OPC is composed of alite, belite and gypsum as well as ferrite which are also observed in Fig. 2. Anhydrous sodium metasilicate powder (Na_2SiO_3) with SiO_2:Na_2O molar ratio at 1:1 was selected as the solid alkaline activator which was provided by Redox Pty Ltd. Tap water was used as the mixing water. Phosphoric acid solution was synthesised by mixing distilled water and analytical reagent-grade ortho-phosphoric acid (85% w/w, 1.71 g/mL), provided by Chem-supply.

Table 1

Chemical compositions of the FA, GGBFS and OPC used (wt.%), as determined by X-ray fluorescence.

Precursor	Component (mass % as oxide)										
	SiO_2	TiO_2	Al_2O_3	Fe_2O_3	MnO	MgO	CaO	K_2O	P_2O_5	SO_3	LOI*
GGBFS	31.00	0.49	13.96	0.32	0.33	6.33	40.92	0.31	0.01	2.17	2.11
FA	42.09	1.44	25.13	13.16	0.18	1.27	13.56	0.41	1.10	0.41	0.81
OPC	20.34	-	4.47	4.58	-	1.24	62.91	0.29	-	2.58	3.27

* LOI refers to loss on ignition at 1,000 ℃.



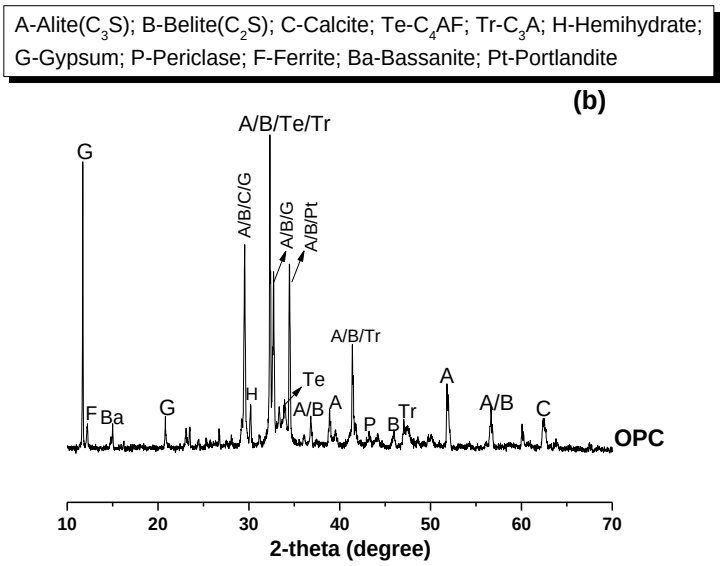


Fig. 1. XRD spectra of the raw materials: (a) Slag and FA; (b) OPC.

2.2. Preparation of AASF and OPC-based pastes

The AASF paste was prepared by mixing the GGBFS and FA dry powders first in a Hobart mixer for two minutes before adding the alkaline activator solution which was made by stirring the Na_2SiO_3 and required water in a beaker, then covered with a watch glass to minimise evaporation and followed by cooling down naturally to room temperature. The mixture was mixed for 8 minutes, cast in two layers into 50 mm cubic moulds or cylinder moulds (Φ 27.5 mm × H 55 mm) and compacted carefully on a vibrating table for two minutes to remove introduced air bubbles during the mixing process. The newly-mixed pastes were cured at 23 ± 2 ℃ with plastic films covered on casting surfaces to minimise moisture loss. After 24 hours, all specimens were demoulded, sealed tightly in plastic bags and stored immediately in a cabinet at room temperature (23 ± 2 ℃) until further testing. For OPC-based pastes, a pilot study was carried out in order to achieve similar compressive strength compared to that of the AASF paste. Pure 100% OPC paste and blended OPC with GGBFS were manufactured with the predetermined water-to-binder ratio at 0.38 and 0.40 respectively. The mixing procedure was similar compared to AASF pastes but the curing condition was different: OPC-based pastes were all cured in water with the same laboratory condition (temperature = 23 ± 2 ℃). Detailed denotations and mix proportions of the three mixes are tabulated in Table 2. Paste samples were used throughout the study and were cured for 56 days to ensure a complete hydration process prior to acid immersions and other tests. It is noteworthy that pastes not mortar or concrete specimens were made for comparison because we mainly deal with the intrinsic

stabilities of different binding components in various binders when suffering from acid attacks without considering interfacial transition zone.

Table 2

Mix proportions of the three types of binder mixes in the study.

Sample code	Composition (%) of the binder	Water/binder ratio	Solid activator dosage (%)
50Slag_50FA	GGBFS: FA = 50:50	0.342	8
65Slag_35OPC	GGBFS: OPC = 65:35	0.40	-
100OPC	OPC: 100	0.38	-

All ratios and percentages are expressed in mass.

2.3. Test procedure

2.3.1. Initial properties before acid immersion

Water absorption accompanied with volume of permeable voids (VPV) and capillary sorptivity of the paste specimens after 56 days of curing[44] were measured according to ASTM C642-06 [45] and ASTM C1585-04 [46], respectively. The preconditioning temperature for the water absorption and VPV, and capillary sorptivity test was 60 ℃ and 50 ℃ respectively because higher temperatures may alter the microstructures of alkali-activated binders [44]. Final results were expressed as an average of three specimens for each mix. The compressive strength after 56-day curing was tested on the 50 mm cubic samples in triplicates using an ELE International tester with a loading rate at 0.9 kN/s in compliance with the ASTM C109/C109M-12 (2012) [47].

2.3.2. Phosphoric acid immersion

In this study, for each binder mix, six cylindrical samples were fully immersed in separated containers with 1 L phosphoric acid (pH = 2.0 ± 0.2) for 44 days and the pH was kept constant by replacing the phosphoric acid solution based on predetermined intervals. Specifically, the solution was replaced every day during the first 7 days and every second day after that until 14 days of immersion. From 14 days, it was renewed every three days until the end of the acid immersion (44 days). The solid surface/liquid volume was approximately 0.29 cm^{-1} and solid/liquid volume ratio was 0.20 throughout the immersion period. The pH level was selected based on the scenarios where concrete structures are applied in sewage wastewater pipes, food process or mining industries [48-50]. The top and bottom surfaces of the specimens were sealed using inert silica gel to ensure a horizontal direction of acid ingress and the corresponding experimental setup can be referred to the literature [8]. Another batch of specimens were

submerged in distilled water as a reference which was also regularly replaced with the same renewal frequency as the phosphoric acid solution. In order to quantify the alkalinity of pore solutions of the three binder mixes, the continuous pH changes over the first day of immersion before renewal of acid or water were monitored using HI 3222 pH/ORP/ISE meter with an accuracy of 0.01. This measurement was only conducted within one day of immersion because the greatest pH changes occur within one-day of immersion [35, 51]. It is worth pointing out that unless further introductions, this exposure regime applies to the samples for all measurements

2.3.3. Degradation kinetic measurements

Degradation depth

Total degradation depth (TDD), simplified as degradation depth was used as the direct indicator of degradation kinetics which is a numerical combination of dissolved/detached depth (DD) [16] due to partial dissolution and/or detachment of specimens in acid solution and apparent degradation depth (ADD) as indicated by phenolphthalein colouration method. A presentation of the TDD, DD and ADD after the spray of phenolphthalein solution is shown in Fig. 2. This method, based on DIN EN 14630:2007-01, has been widely used as a reliable indicator of various degradation processes [36, 52-55]. The detailed description of the degradation depth measurement is introduced in the following references [8, 24]. The measurements were conducted on small disks cut from 6 parallel specimens which were continuously submerged in the acid solution throughout the entire immersion period.

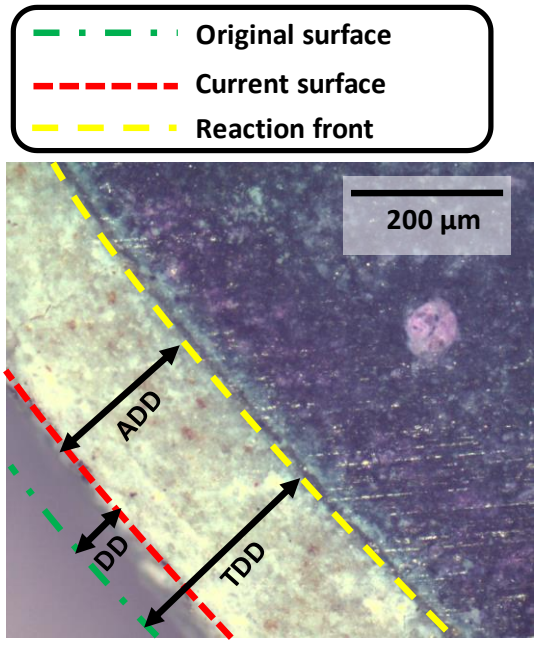


Fig. 2. An image of a disk-shaped sample cross-section after phenolphthalein spray showing the determination of total degradation depth (TDD), ADD and DD.

Mass changes

Mass changes were examined before each measurement of degradation depth. At each sampling stage, specimens were taken out from the phosphoric acid solution gently and dried slightly using a wet cloth before weighing to remove surface water. The whole weighing process was completed within 30 seconds to minimize the water evaporation from sample surfaces using a digital scale with a precision of ± 0.01 g. Samples were then positioned back into the phosphoric acid solutions. At the same time, mass changes of the references submerged in distilled water were also recorded.

Leaching rates of related ions

Concentrations of different elements including Ca, Na, Al and Si in the phosphoric acid solution were analysed by Inductively coupled plasma-optical emission spectrometer (ICP-OES) analyser (Optima 4400, Perkin Elmer, USA). Three cylindrical samples (Φ 27.5 mm × H 55 mm with volume of 32.65 cm^3) of each mix was immersed in 900 mL phosphoric acid solution separately with the same pH level (2.0 ± 0.2). The solid/liquid volume ratio was 0.11 for all mixes because a higher ratio could lead to the concentrations of ions above the testing limits. The renewal of acid occurred right after 3, another 4 (7 days in total), another 3 (10 days in total), and another 4 (14 days in total) days of immersion, the frequency of which was lower than that of the degradation depth measurements because of a smaller solid/liquid volume ratio used in this test. The concentrations of Ca, Na, Al, Si, released out from the specimens in the corresponding leachate phosphoric acid solutions were measured right before each renewal of acid, namely after a total of 3, 7, 10 and 14 days as well as 21 days by the end of the immersion.

2.3.4. Mineralogical, chemical and microstructural analysis

Mineralogical and chemical characteristics of both degraded and undegraded part of specimens were evaluated using X-ray diffraction analysis (XRD), thermogravimetric analysis (TGA), derivative thermogravimetry (DTG) and environmental scanning electron microscope equipped with energy dispersive X-ray spectroscopy (ESEM/EDS). Micro X-ray computed tomography (μ-XCT) was also used to provide non-destructive three-dimensional (3D) microstructural information on the degraded and undegraded regions of the specimens.

Crushed samples from both degraded and undegraded parts of the specimens after 44-day immersion were grounded into fine powders (passing through the 75 μm sieve (No.200)) followed by drying in a desiccator for 24 hours at room temperature prior to XRD and

TGA/DTG tests. For ESEM/EDS, samples after 14-day immersion were first pre-heated at 60 ℃ for 48 hours to expel all moisture and then sectioned including both degraded and undegraded part, impregnated with epoxy resin and polished using SiC abrasive paper prior to the analysis. The 3D microstructures of a piece of specimens cut off from the sample surface after 21-day immersion were examined using XCT. The dimension of each binder mix was around 1 mm in width and length to obtain a high resolution (1.77 μm). The 14-day and 21-day testing point was selected because the degradation performance is discernible enough after these immersion periods, shortly after the induction stage for the 50Slag_50FA sample.

XRD patterns were recorded using a Bruker D8 Advance diffractometer with Cu – Kα radiation and data were collected in a 2θ range of 10-70°. The scanning rate was 1.2°/min. TGA/DTG was carried out in a PerkinElmer Diamond instrument. ESEM was conducted using an FEI Quanta instrument with a 15 kV accelerating voltage and the working distance was 10 mm. EDS was run by a Link-Isis (Oxford Instruments) X-ray energy dispersive detector for chemical composition analysis. Micro-CT analysis was performed with a Phoenix Nanotom m (Waygate Technologies) operated using xs control and Phoenix datos|x acquisition reconstruction software (both Waygate Technologies). Micro-CT scans were collected over 47.5 minutes using an x-ray energy of 60 kV and 240 uA collecting 1400 x-ray projections through a full 360 degrees of rotation. Reconstructed data was exported in a 16-bit format and imported to Avizo (Thermo Fisher Scientific) for analysis.

2.3.5. Intrinsic acid resistance measurement

In order to eliminate the influence of porous structure on the acid resistance of different cementitious binders, specimens were ground to fine powders (size < 90 μm). Then they were immersed in a nitric acid solution (approximately 0.06 wt.%, pH = 2.0 ± 0.2) to avoid possible clogging effect that may happen to other acids because nitrates are highly soluble without any precipitation [56]. For each mix, 0.2 g powders were firstly immersed in 200 mL nitric acid solution and then constantly stirred for one minute followed by natural deposition in ambient environment. This small amount of powder but large volume of acid solution was employed to avoid the need for acid renewal due to pH changes. After 48-hour immersion, three suspension solutions for different mixes were vacuum filtered by gravity filter paper (8 μm in pore size). The powders on the filter paper were then rinsed with deionised water completely until a neutral pH was obtained. After that, the insoluble residue powders were dried at 50 ℃ for at least 3 days to remove any moisture until a constant mass was achieved. Finally, the residue powder was weighed to calculate the dissolution rate (DR) using the following equation:

$$DR = \frac{M_{before} - M_{after}}{M_{before}} \quad (1)$$

where M_{before} and M_{after} refers to the mass before immersion and the dry mass of residual powders respectively. In this study, M_{before} is approximately 0.2 g for all binder mixes. The measurement was repeated twice.

Since the dissolution rate is highly dependent on the surface area of reactants [57], the surface area of the initial powdered sample after 56 days of curing was also quantified by performing Brunauer-Emmett-Teller (BET) analysis in compliance with ISO 9277 [58]. Powdered samples were first preconditioned by outgassing, drying under vacuum at 150 ℃ for 24 hours [59]. Then their surface areas were analysed using nitrogen absorption/desorption method [60]. It is worth mentioning that the small amount of samples (around 0.2 g) but higher volume of nitric acid solution used could minimise the possible neutralisation effect of powdered samples.

3. Results and discussion

3.1. Basic properties before acid immersion

The basic properties of the three mixes prior to the acid exposure are shown in Table 3. From Table 3, it is clear that all specimens obtained similar compressive strength (62 ± 3 MPa) before immersion. 65Slag_35OPC and 50Slag_50FA had the highest and lowest water absorption and VPV respectively, due to their largest and lowest amount of mixing water used (Table 2) accordingly. However, 65Slag_35OPC pastes displayed the lowest capillary sorptivity despite of its highest water absorption and VPV. This might be explained by considering its porous structure changes during the 56-day curing period. Due to the largest amount of mixing water used, many pores were left in the binder matrix after water evaporation, leading to the highest water absorption and VPV [2]. However, the late hydration process of this paste due to partial replacement of OPC by GGBFS refined its porous structures [61], leading to the formation of many isolated pores which reduced the continuity of pore structures. Thus, a low capillary sorptivity was obtained. As a higher rate of water ingress caused by capillary forces indicates a higher susceptibility of early-stage acid attacks as water is the vehicle of aggressive ions, it suggests that 50Slag_50FA and 100OPC are more vulnerable towards acid attacks compared to 65Slag_35OPC from the perspective of porous media [2].

Table 3

Basic properties of the paste samples used in this test prior to the immersion in the phosphoric acid attack.

Sample ID	Water absorption (%)	VPV (%)	Capillary sorptivity (mm/min^0.5)	Compressive strength (MPa)
50Slag_50FA	17.7 ± 0.1	29.3 ± 0.2	0.36 ± 0.03	64.33 ± 5.78
65Slag_35OPC	26.6 ± 0.1	38.4 ± 0.1	0.14 ± 0.05	59.90 ± 6.44
100OPC	19.6 ± 0.3	31.3 ± 0.4	0.33 ± 0.01	64.92 ± 3.78

VPV-Volume of permeable voids.

3.2. Degradation kinetics

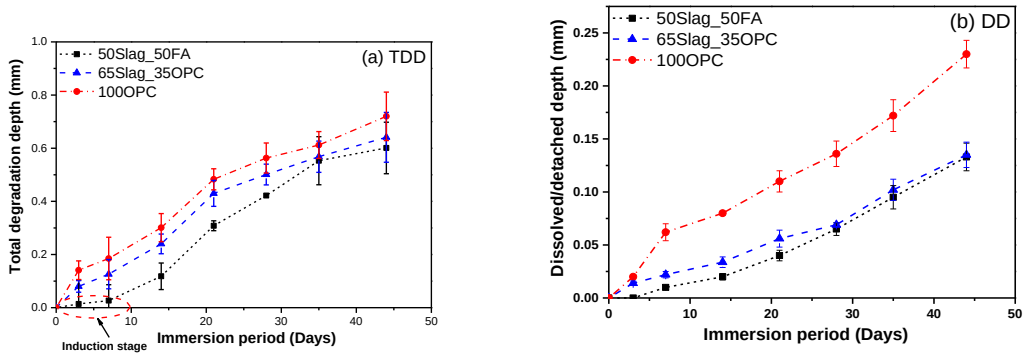
3.2.1. Degradation depth

The degradation depths, including TDD, DD and ADD of all mixes exposed to the phosphoric acid solution within 44 days of immersion are shown in Fig. 3(a)-(c). From Fig. 3(a), the TDD of 50Slag_50FA specimen was less than that of the two OPC-based counterparts throughout the immersion period, especially within about 0-14 days. Besides, it seems that 50Slag_50FA specimen displayed an induction stage within 7 days of immersion with very little degradation depth measured as highlighted in a red dash circle. After 7 days, the TDD of 50Slag_50FA increased considerably until 35 days followed by a lower rate of increase until the end of the 44-day immersion with final TDD at 0.60 mm. In contrast, the 65Slag_35OPC had an almost linear increase in TDD first within 21 days and then the TDD increased at a lower rate until the end of exposure. 100OPC followed a similar trend as that of 65Slag_35OPC but with larger TDD throughout the whole immersion period. After 44 days of immersion, the TDD of 65Slag_35OPC and 100OPC was 0.64 and 0.72 mm respectively.

For DD values (Fig. 3(b)), 50Slag_50FA and 65Slag_35OPC specimens exhibited similar trends, increasing almost linearly against immersion period with the DD of 65Slag_35OPC slightly larger. In comparison, 100OPC had a much larger DD over the entire immersion period compared to the other two binders. This significant difference can be explained by considering the different intrinsic chemical stability of main components in the binder matrix: portlandite [$Ca(OH)_2$], ettringite and C-S-H gel (the main hydration products in 100OPC binder) can be dissolved and/or decomposed completely by acid attacks via decalcification process when pH is around 3 or lower regardless of acid types [62]. As C-S-H gel is the main contributor to the strength of OPC-based binders [63], accounting for 60%-75% of the total volume of paste [64, 65], its dissolution and decomposition can thus result in almost complete disintegration of the whole binder matrix (evidenced by the largest DD). However, due to higher contents of Al but lower contents of Ca in GGBFS and FA compared to OPC (Table 1), the binding gels formed in 50Slag_50FA or 65Slag_35OPC have more Al and less Ca compared to 100OPC. It is confirmed that gels with more Al are more stable and resistant towards decalcification due to

their more intensely cross-linked networks [66]. Besides, Al and Si have a higher pH stability, or greater ability to not leach out of binder at a certain pH, compared to Ca [54]. These explain why 50Slag_50FA and 65Slag_35OPC obtained much less DD compared to 100OPC.

From Fig. 3(c), 50Slag_50FA had very little ADD within the 7 days of immersion (also marked as 'induction stage') followed by a significant rise from 7-35 days. 65Slag_35OPC and 100OPC samples obtained similar ADD values with a seemingly proportional increase over the immersion period. After 44 days, the ADD was 0.47, 0.51 and 0.49 mm for 50Slag_50FA, 65Slag_35OPC and 100OPC respectively. Different ADD are closely associated with available OH^- (hydroxyls) in the binder matrix based on its definition: if the pore solution of binder matrix has a high concentration of OH^- that can neutralise H_3O^+ from the acid solution, the pH of the pore solution can maintain relatively stable for a certain period. However, if the concentration of OH^- is not high enough to neutralise H_3O^+ or they are neutralised at the expense of the formation of many cracks near the sample surface, the pH of the pore solution would decrease rapidly. Hence, the delayed ADD evolution of 50Slag_50FA evidenced by the induction stage suggests it has a large reservoir of soluble and mobile alkalis which prevent a sudden drop in the pH of AASF pore solutions [67]. In comparison, the instant response of pH increment implies that the two OPC pastes either had a lower concentration of OH^- in the pore solution and/or the binder matrix was severely disintegrated, thus providing almost no extra 'protection' against the acid penetration.



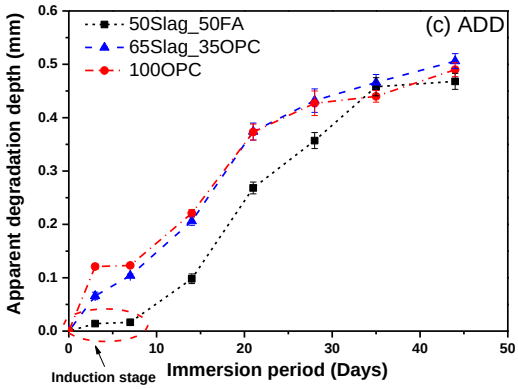


Fig. 3. The (a) TDD, (b) DD and (c) ADD of the three cementitious pastes exposed to the phosphoric acid (pH = 2.0 ± 0.2) over 44-day of immersion.

To confirm this, the pH evolutions over the first day of immersion in phosphoric acid and water are shown in Fig. 4. It is apparent that 50Slag_50FA led to a greater increase in the pH of the corresponding solutions compared to that of the OPC-based peers both in the phosphoric acid and in water, suggesting that it has a stronger neutralisation capacity. Considering the least ADD of 50Slag_50FA, it seems to have an ability to maintain the pH of pore solution at a high level (pH > 8.3) because of a large reservoir of OH^- that is readily available to neutralise external H_3O^+ ions. This result corresponds well with the other studies [51, 67] which reported that the concentration of OH^- in the pore solution of one type AASF with the same slag/FA ratio is more than 1000 mmol/L, indicating a pH higher than 14. Besides, bound alkalis provide the AAMs with a large reservoir of exchangeable cations to prevent a sharp drop in the pH of pore solutions. However, the pH of the pore solutions of OPC binders is relatively lower, ranging between 12.5 and 13.5 [68-70] and that's why OPC-based binders had larger ADD than that of the 50Slag_50FA paste. The significant increase in the ADD of 50Slag_50FA after 7 days reveals that most of the OH^- available were almost consumed. The final slightly larger ADD for 65Slag_35OPC than 100OPC is consistent with the former's smaller increase in the pH in Fig. 4(a) and (b). This is because 100OPC has a large amount of Portlandite which is able to consume H_3O^+, also known as the buffer effect [71].

In conclusion, the 'induction stage' in ADD and TDD is closely associated with the higher neutralisation capacity of the 50Slag_50FA specimen, providing a buffering effect during the early stage.

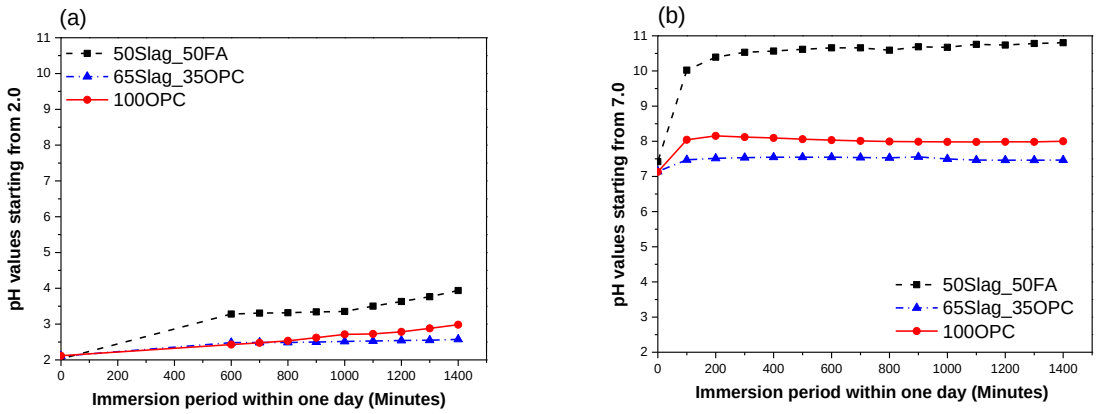


Fig. 4. The pH variations of (a) phosphoric acid solution and (b) water solution within the first day of immersion.

3.2.2. Mass changes

Fig. 5 presents the mass changes of the three binder mixes in the phosphoric acid and in water as reference over the early-stage immersion period. The obvious initial mass gain for all binder mixes regardless of phosphoric acid solution or water is due to water absorption and similar results were also reported in previous studies [72, 73]. After a certain period, mass losses were observed for specimens exposed to phosphoric acid whereas a slight mass increase or a constant mass was observed for 50Slag_50FA and OPC-based binders respectively for the immersion in water.

For immersion in the phosphoric acid, 50Slag_50FA experienced the largest mass increase (2%) after about three days followed by a decrease in mass gain up to about 24 days. After that, the actual mass loss occurred with the final mass loss at 0.79% by end of the immersion. The largest mass increase for 65Slag_35OPC and 100OPC sample was 0.34% and 0.54% respectively after 3-day immersion, much smaller than that of the 50Slag_50FA. An apparent mass loss compared to the initial value was observed after about 10 days for the two OPC-based mixes, about 14 days earlier compared to the 50Slag_50FA. The highest mass gain and delayed mass loss for the 50Slag_50FA might be associated with its highest capillary sorptivity (Table 3), relatively stability of binding components and possible precipitations of some reaction products. For 65Slag_35OPC sample, the mass loss decelerated gradually whereas the mass loss decreased almost constantly for 100OPC. The final mass loss of the two was 1.35% (65Slag_35OPC) and 2.09% (100OPC).

In conclusion, the mass losses of the three mixes were consistent with the degradation depths, with an increasing order at 50Slag_50FA < 65Slag_35OPC < 100OPC. It is worth noting that the much greater mass gain owing to acid solution ingress for the 50Slag_50FA but

similar starting point of the loss in mass gain at about 3 days for all mixes suggest that this binder is more resistant towards mass losses due to this acid attack compared to the OPC-based peers. It is suggested to use fully-saturated specimens before immersion in acid solutions to avoid misleading mass gains caused by the ingress of acid solutions.

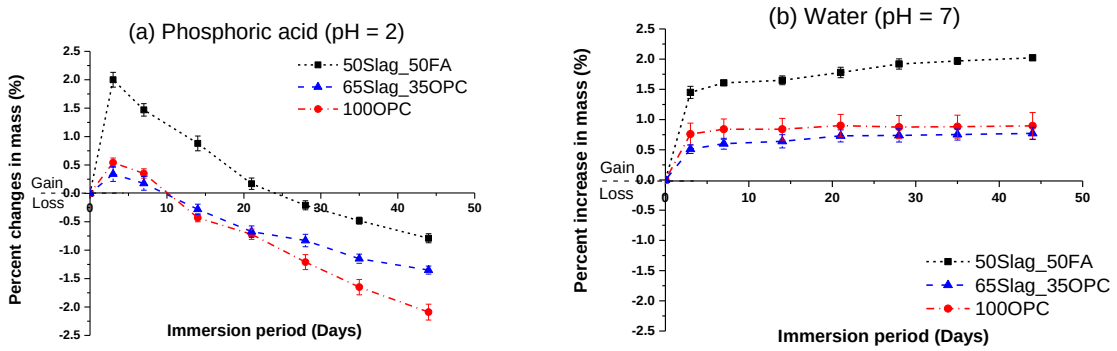


Fig. 5. Mass changes over 44-day immersion time for the three binder mixes in (a) phosphoric acid and (b) water.

3.2.3. Leaching rates of related elements

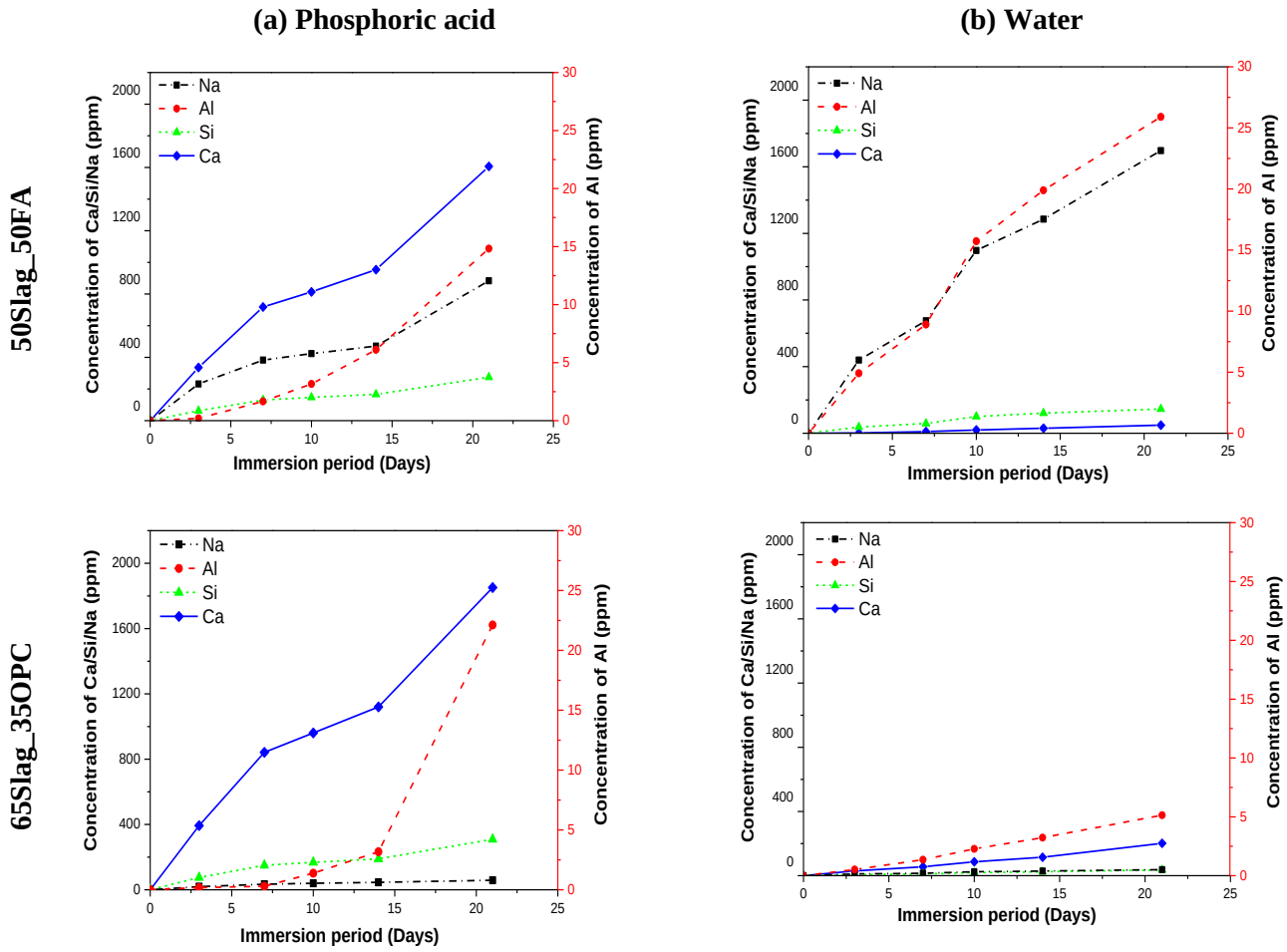
The leaching behaviour the related elements released from the three mixes during 21 days of immersion in the phosphoric acid and in water are depicted in Fig. 6. The cumulative concentration of Na, Ca, Al and Si is denoted as [Na], [Ca], [Al] and [Si] respectively hereafter. Due to insignificant contents of Na in the OPC-based binders, [Na] is not discussed for OPC-based binders.

During immersion in the phosphoric acid, a remarkable increase in [Ca] can be observed for all mixes compared to the [Si], [Al] or [Na]. For instance, the [Ca] was 1606.6 ppm for the solution containing 50Slag_50FA, which was even higher than the total sum of [Si], [Al] and [Na] (1172.7 ppm). This phenomenon is attributed to the high content of Ca in all mixes and higher neutralisation capacity of bivalent Ca^{2+} ions compared to monovalent Na^{+}. 50Slag_50FA also led to a large [Na] which was 883.4 ppm owing to the sodium-based alkaline activator used while making the specimen. The high [Ca] and [Na] are in line with the highest neutralisation capacity and the presence of ‘induction stage’ for 50Slag_50FA because these counter-balancing ions are accompanied with a lot of OH^{-}, maintaining the pH value of the pore solution for a while without considerably affecting the stability of the binding phase. The [Al] and [Si] for 50Slag_50FA were much lower, which was 14.8 ppm and 274.5 ppm respectively. Similarly, the corresponding value was 22.1 and 309.0 ppm for 65Slag_35OPC, 5.4 and 208.5 ppm for 100OPC respectively. All of these suggest that Al and Si are less sensitive compared to Ca when exposed to the acid attack [54]. It is worth noting that for all

mixes, the release of Al seemed to be curbed probably because of the relative high stability of Al-bearing phases, such as C-(N)-A-S-H in the 50Slag_50FA and calcium aluminate phases in OPC-based binders [19, 74].

Compared to the [Ca] in the phosphoric acid, [Ca] in water was much lower irrespective of binder mixes indicating that Ca is quite sensitive to H_3O^+ induced by the acid solution. In addition, the [Na] and [Al] in water for 50Slag_50FA was higher due to their high mobility, especially for Na. The OPC-based two mixed binders had similar [Al] and [Si] which increased almost linearly with an increase in the immersion periods.

In summary, Ca is much more sensitive towards H_3O^+ compared to Si and Al, corresponding well with the results from other research [75, 76]. Moreover, apart from Ca, 50Slag_50FA can release a large amount of Na which plays an important role in consuming H_3O^+ ions produced by acid solutions and maintaining a stable pH of the pore solution.



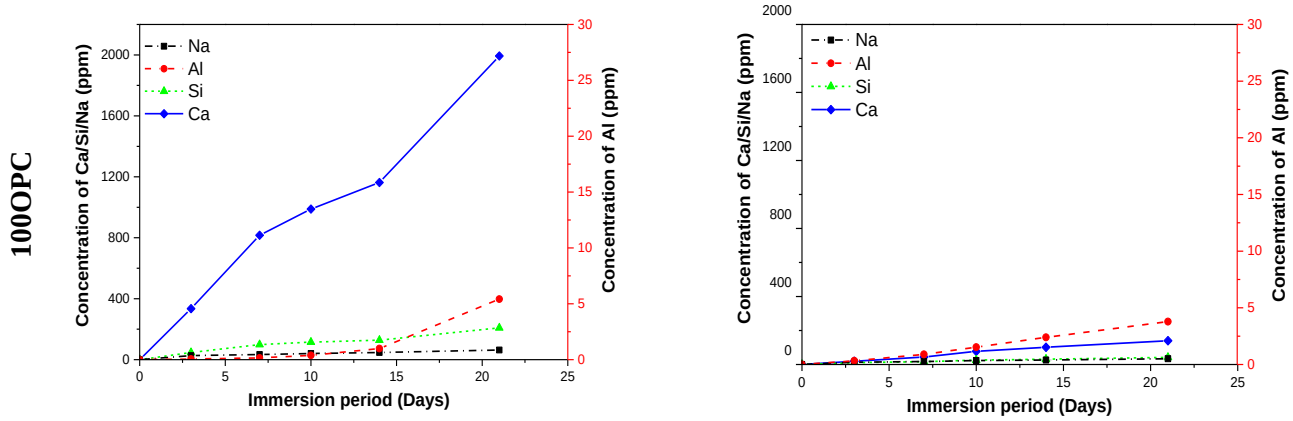


Fig. 6. Cumulative concentrations of different elements in the two solutions released from the three mixes within 21 days of immersion, (a) Phosphoric acid; (b) Water.

3.3. Microstructural characterisation

3.3.1. Mineralogy

X-ray diffraction (XRD)

Fig. 7 shows the XRD spectra of the three mixes after 44 days of immersion in the phosphoric acid solution. Based on Fig. 7(a), it can be seen that due to the acid attack, major components such as Ca-bearing gismondine ($CaO{\cdot}Al_2O_3{\cdot}2SiO_2{\cdot}4H_2O$ PDF # 00-002-0096) and C-(N)-(A)-S-H (a type of calcium silicate hydrate substituted by Al and Na) [39, 77-79] which are present in the undegraded part of 50Slag_50FA all disappear. Quartz (PDF # 00-001-0649) and mullite (PDF # 00-001-0613), however, still appear due to some unreacted FA in the degraded part. This result implies that the phosphoric acid attack resulted in decalcification of the main binding gels in the 50Slag_50FA paste along with dealkalisation and dealumination. The dealkalisation and dealumination were also verified by the leaching results of Al and Na in Fig. 6. Moreover, some phosphates were identified in the degraded part, such as Brushite ($CaHPO_4{\cdot}2H_2O$ PDF # 00-001-0395) and sodium phosphate hydrate oxide ($Na_2HPO_4{\cdot}12H_2O$ PDF # 00-001-0223). The formation of Brushite was also reported in another study [1] due to silage effluent attacks as silage effluents also contain phosphates. Possible chemical reactions are shown below:

$$Ca^{2+} + HPO_4^{2-} + 2H_2O \rightarrow CaHPO_4{\cdot}2H_2O \text{ (Brushite)} \quad (1)$$

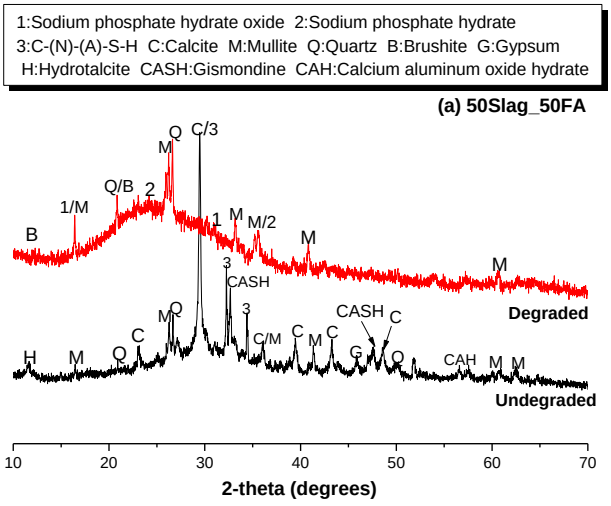
$$2Na^{+} + HPO_4^{2-} + 12H_2O \rightarrow Na_2HPO_4{\cdot}12H_2O \quad (2)$$

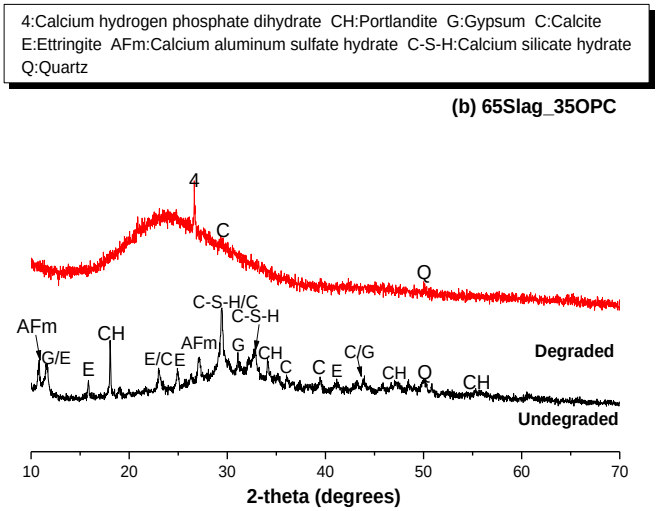
Fig. 7(b) and (c) shows that Portlandite ($Ca(OH)_2$ PDF # 00-001-1079), C-S-H gel (PDF # 00-002-0068), calcite ($CaCO_3$ PDF # 00-001-0837) and ettringite ($Ca_6Al_2(SO_4)_3(OH)_{12}{\cdot}26H_2O$ PDF # 00-002-0059) are main phases in the OPC-based binding matrix without acid attacks.

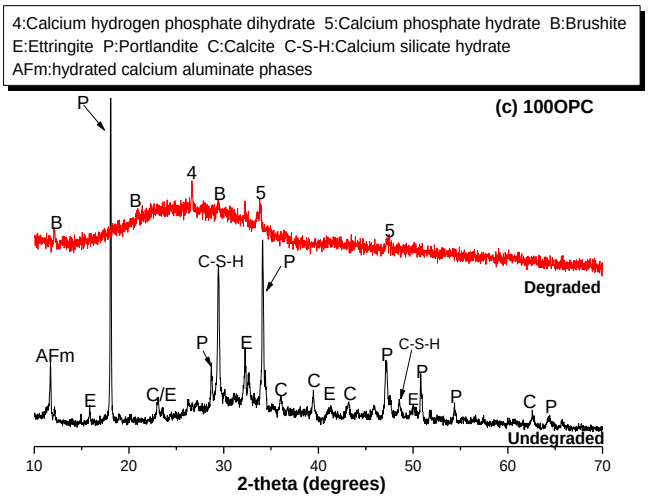
However, all of these phases disappear in the corresponding degraded parts, indicating their vulnerability to the phosphoric acid [74]. For 65Slag_35OPC, minor traces of quartz (PDF # 00-001-0649) and calcium hydrogen phosphate dihydrate ($CaHPO_4 \cdot 2H_2O$ PDF # 00-001-0653) were detected in the degraded part. Brushite ($CaHPO_4 \cdot 2H_2O$ PDF # 00-001-0395) and a type of calcium phosphate hydrate ($Ca(H_2PO_4)_2 \cdot H_2O$ PDF # 00-001-0471) can be observed in the degraded part of 100OPC binder. The presence of the $Ca(H_2PO_4)_2 \cdot H_2O$ can be explained by the reaction below that could happen in the interstitial solution or at the surface of the sample:

$$Ca^{2+} + 2H_2PO_4^- + H_2O \rightarrow Ca(H_2PO_4)_2 \cdot H_2O \quad (3)$$

It is also noticed that after the phosphoric acid immersion, a wide halo is present in degraded parts of all mixes (extending from around 15 to about 35° 2θ). These can be ascribed to the formation of amorphous phases due to acid attacks [19]. The wider and more flattened halo of 100OPC sample than the other two binders indicates a more severely degraded part, consistent with the highest degradation kinetic of 100OPC.







458

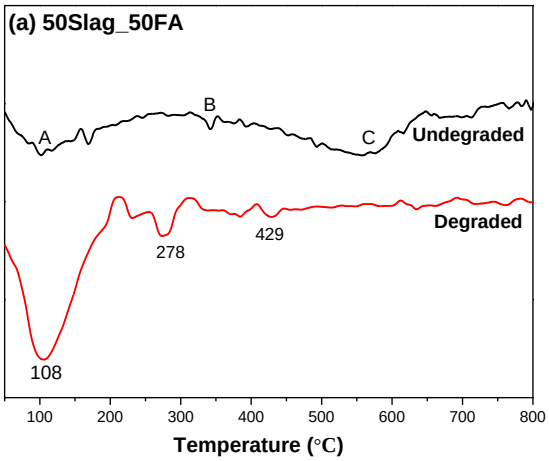
459 **Fig. 7.** XRD patterns of the three mixture pastes (a) 50Slag_50FA; (b) 65Slag_35OPC and (c)
460 100OPC including both degraded and undegraded parts after 44-day immersion period in the
461 phosphoric acid (pH = 2.0 ± 0.2).

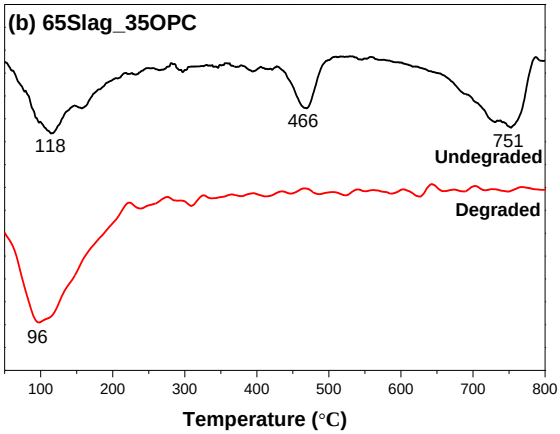
462 ***Differential Thermogravimetry (DTG)***

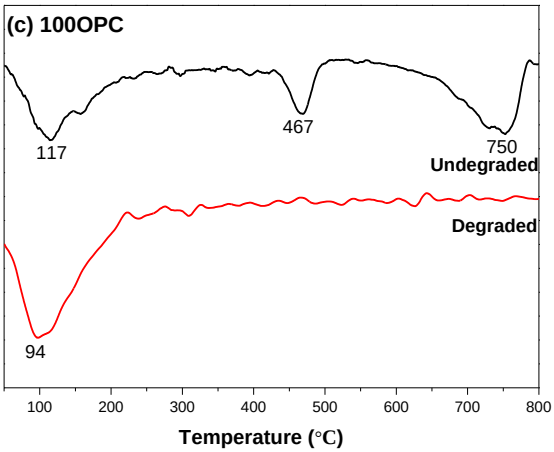
463 DTG curves of the three binder mixes including degraded and undegraded part of specimens
464 are shown in Fig. 8. Table 4 lists the characteristic peak attributions for all the curves. It can be
465 observed that there are three small peaks marked as 'A', 'B' and 'C', belonging to evaporable
466 water or moisture loss from 50Slag_50FA undegraded binding matrix [80-82] , decomposition
467 of C-A-S-H and C-A-H [83-85] and decomposition of carbonates (e.g. calcite) [86, 87],
468 respectively. In comparison, no 'B' and 'C' peaks could be observed in the degraded part.
469 Rather, two obvious peaks located at 278 and 429 ℃ are present which might be associated
470 with the formation of calcium phosphates, as verified in XRD patterns. Besides, a significant
471 mass loss exists at around 108 ℃, indicating that more water (loosely bound or unbound) is
472 evaporable after the acid attack due to the transformation of many original crystalline phases
473 to amorphous ones, as shown in Fig. 7(a).

474 For the undegraded part of the OPC-based binders, the first mass occurring at 118 ℃ and
475 117 ℃ respectively for 65Slag_35OPC and 100OPC can be assigned to the loss of evaporable
476 free water, dehydration of C-S-H gel and ettringite [80, 81, 88]. The peaks centered at 466 and
477 467 ℃ for 65Slag_35OPC and 100OPC respectively are due to the dehydroxylation of
478 Portlandite [81]. The last significant mass loss located at around 750 or 751 ℃ is attributed to
479 the decomposition of carbonate minerals, such as calcite [89, 90], in accordance with the XRD
480 results. Similar to XRD, corresponding peaks assigned to Portlandite and calcites are not
481 present in the DTG curves of the degraded part. The only obvious mass loss located at lower
482 temperatures, 96 ℃ (65Slag_35OPC) and 94 ℃ (100OPC), compared to those in the

undegraded part, indicates the presence of a larger amount of less tightly bound water. This is in large part due to the formation of some less crystalline and amorphous phases such as silica-gel after the phosphoric acid immersion, corresponding well with the wide halo in the XRD results. It is noteworthy that no phosphates are noticeable in OPC-based DTG curves, probably because the total amount of these phosphates are too small to be detected or most of them were dissolved in the acid solution. Based on the XRD results which show traces of calcium phosphates, it is highly possible only a little amount phosphates were left in the degraded layer of OPC binders.







494

495 **Fig. 8.** DTG curves of the three mixes including degraded and undegraded part of the specimen.

496 **Table 4**

497 Temperature ranges within or at which corresponding changes in phases take place.

Different phases and changes	Temperature ranges (℃)	References
Loss of evaporable water	0–120, usually < 100	[80, 81]
Removal of the moisture within C-S-H type gel	50-200	[91, 92]
Loss of water in N-A-S-H	≈ 100	[82]
Loss of bound water in C-(A)-S-H	30-650	[91]
Decomposition of ettringite	114-116/110-170/104-114	[93, 94]/[81]/[95]
Mass loss of AFm phases	146	[96-99]
Dehydroxylation of calcium hydroxide	450-550/430-520	[81, 95, 100]/[86]
Decomposition of carbonates	560-700/741-797	[86, 87]/[89, 90]

498

499 **3.3.2. Microstructure**

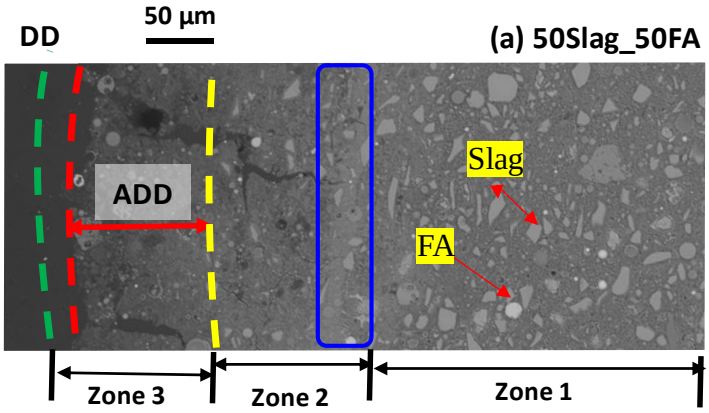
500 ***ESEM and EDS***

501 SEM images in backscattering mode and elemental distributions of the three mixes after 14
502 days of immersion are shown in Fig. 9 and Fig. 10 respectively. The corresponding DD and
503 ADD obtained from Fig. 3 are also marked. The DD of the 50Slag_50FA, 65Slag_35OPC and

100OPC was 20.0, 33.8 and 80.0 μm respectively and the corresponding ADD was 96.6, 206.2 and 188.4 μm respectively.

In Fig. 9, it is clear that three zones can be identified for all the samples: Zone 1 represents the undegraded part of the samples with brighter grey colour compared to other regions as it contains many unhydrated OPC particles for OPC-based binders or unreacted GGBFS and FA particles for 50Slag_50FA [72, 101]. Zone 2 is a transition zone starting from a bright grey narrow strip (partitioned as blue solid line frames) which should be a region rich in phosphates (as discussed later) to the right boundary of ADD (yellow dashed line, also considered as the 'reaction front'). In this zone, both obvious cracks (closer to surface) and unreacted/unhydrated particles exist. Zone 3 is composed of DD and ADD with many microcracks and voids, indicating a severe degradation result.

The most distinct part is Zone 2 of 50Slag_50FA compared to that of the other OPC-based pastes. Firstly, the width of the narrow strip is apparently larger indicating more precipitations of phosphates, in accordance with the mineralogical analysis (shown in Fig. 8(a)). Additionally, 50Slag_50FA has a thicker Zone 2, implying a stronger resistance to the ingress of H_3O^+ ions as they need to penetrate this zone first before attacking new undegraded areas. This is critical for maintaining high resistance towards acid attacks. This thicker zone 2 has also been reported in previous studies [19, 102].



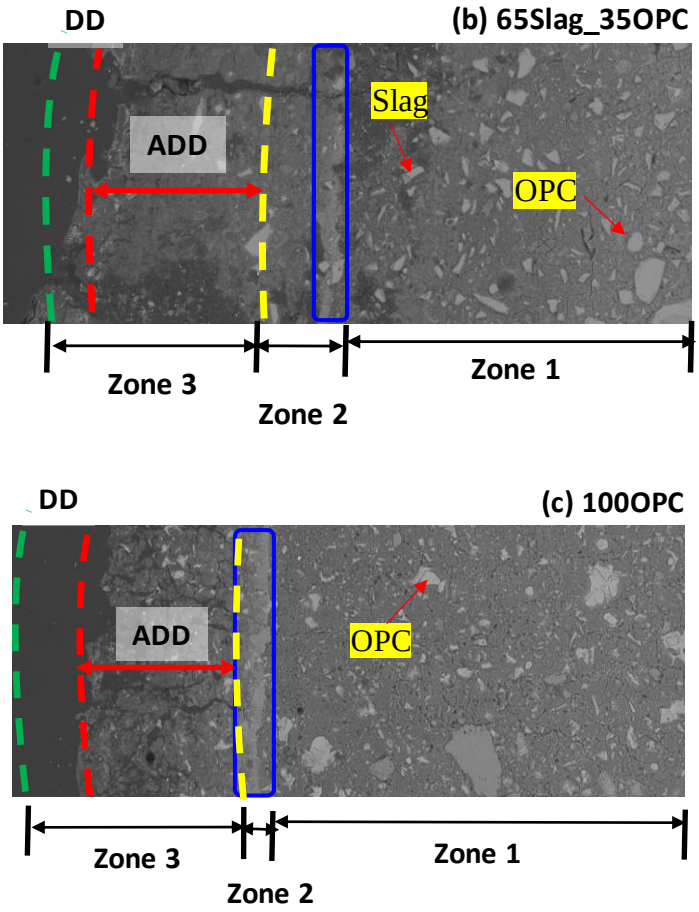
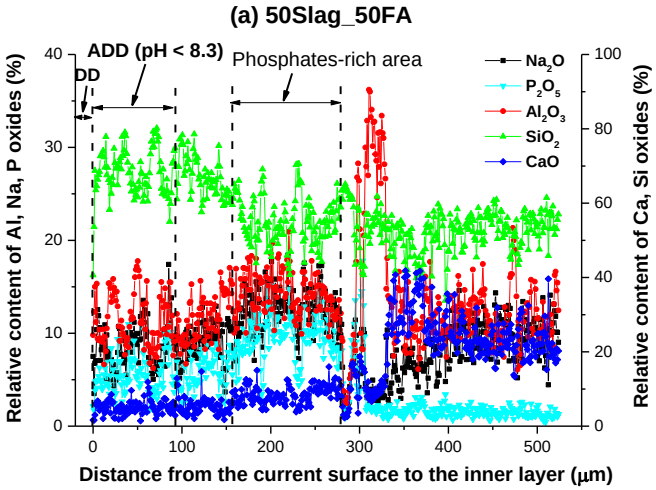


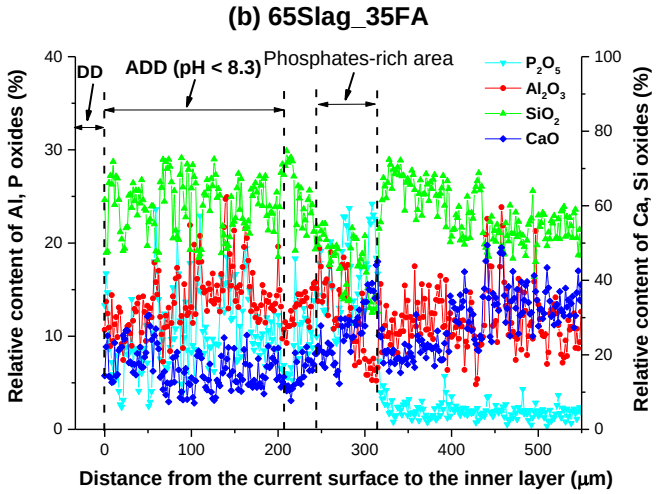
Fig. 9. SEM images of the paste samples (a) 50Slag_50FA; (b) 65Slag_35OPC and (c) 100OPC after 14 days of immersion in the phosphoric acid.

The elemental distributions from the surface to the inner part of the specimens are shown in Fig. 10. Consistent with the locations of the blue solid line frames in Fig. 9, a much higher phosphorus concentration is observable implying the precipitations of different phosphates. A closer examination shows that the phosphates-rich area of 50Slag_50FA is located farther from the reaction front followed by that of 65Slag_35OPC and 100OPC. For all mixes, the relative concentration of Ca decreased as approaching to the degraded surface while Al and Si displayed the opposite trend, in agreement with the leaching behaviour of these elements, which demonstrates that Ca is more sensitive towards acid attacks compared to Al and Si.

50Slag_50FA encountered an increase in the relative concentration of Al accompanied with a decrease in the Ca and Na relative content. This can be explained by the ease of ion exchanges of Ca and Na with H_3O^+ compared to Al, in line with the delayed leaching behaviour of Al as shown in the ICP-OES analysis and other studies [103]. It seems that Al is much less mobile in AAM binding gels because according the previous studies, more Al are in coordinate 3 (q^3) than in coordinate 2 (q^2) [104, 105] in these systems, giving them a better stability toward acids

compared to Na and Ca [106]. The higher concentrations of Al and Si also confirms an aluminosilicate type gel formed in the degraded area. In contrast, OPC-based pastes had no such sharp increase in the relative concentration of Al and the changes of Ca or Al were relatively stable.





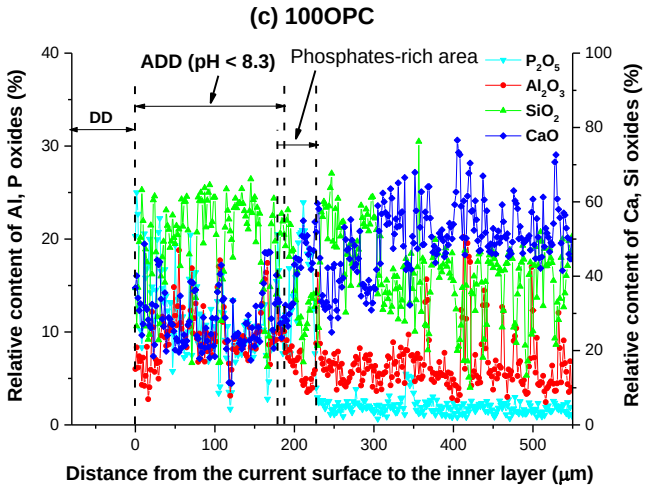


Fig. 10. Chemical analysis of different elements relative content measured by EDS line scan after 14 days of immersion in the phosphoric acid, (a) 50Slag_50FA; (b) 65Slag_35OPC and (c) 100OPC.

Micro-CT analysis

Three dimensional images of the three mixes after 21 days of acid immersion are shown in Fig. 11 and corresponding ADD and DD values based on Fig. 3 are also provided. Similar to SEM images, light-grey areas refer to undegraded components with fewer pores and more unreacted particles (higher density) whereas darker grey areas represent phases containing more pores and fewer unreacted particles (lower density) meaning they are already partially or completely degraded. The resolution was 1.78 μm in this study.

For 50Slag_50FA and 65Slag_35OPC samples, it is apparent that the binders remain more or less undegraded (light grey) even when the pH is lower than 8.3 (within the 'ADD' area), which is not the case for 100OPC. Oppositely, the 100 OPC sample displayed some degraded parts where the pH is still above 8.3 (outside of 'ADD' area). This result is in consistent with the pH stability of different components in the corresponding binders. For 100OPC, the main components including $Ca(OH)_2$, ettringite and C-S-H all disappear when pH is lower than 10.5 and thus degraded part is present even when pH is still above 8.3 [26]. In comparison, less soluble and mechanically sound aluminosilicate gel even after exposure to acids with pH at 3 [27, 107] in 50Slag_50FA and 65Slag_35OPC (also rich in C-(A)-S-H) explains why phases within 'ADD' were still stable. A light grey layer can be observed in the degraded part of the two OPC-based binders, which is assumed to be different phosphates.

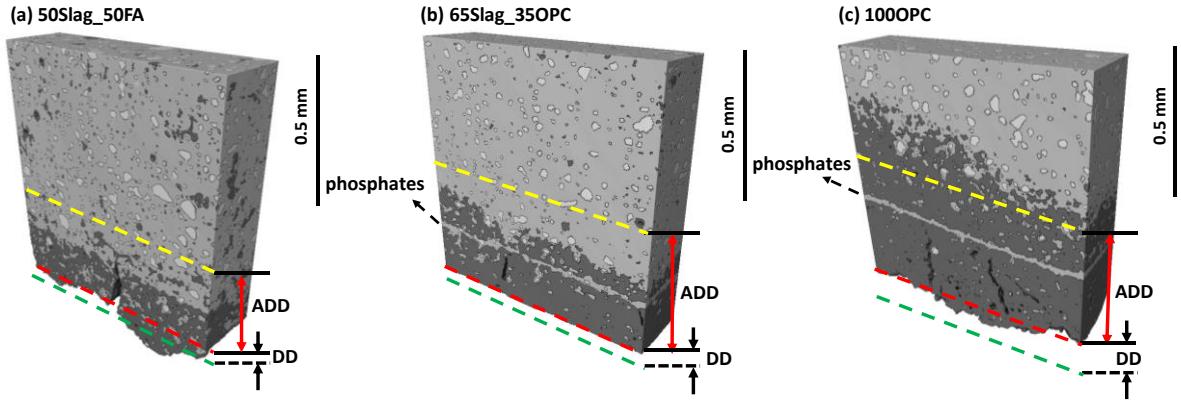


Fig. 11. 3D micro-CT images of the samples after 21-day exposure towards the phosphoric acid: (a) 50Slag_50FA; (b) 65Slag_35OPC and (c) 100OPC. DD and ADD are also labelled based on the experimental results. Green dashed lines refer to the original surfaces of pastes.

Different volume fractions of the phases in the corresponding mixes based on the 3D images after segmentation and data processing procedure are presented in Fig. 12. The four types of components are determined based on their different relative densities obtained from Fig. 11. ADD values are also included to correlate different components with pH values of pores. The number '1', '2' and '3' indicate the main location of the precipitated phosphates because the undegraded binder experienced an abrupt increase in volume fraction as approaching to the surface which is assumed to be the phosphates with a higher density than the degraded binder. It is also apparent that the undegraded binder maintained a certain volume even within the 'ADD' region.

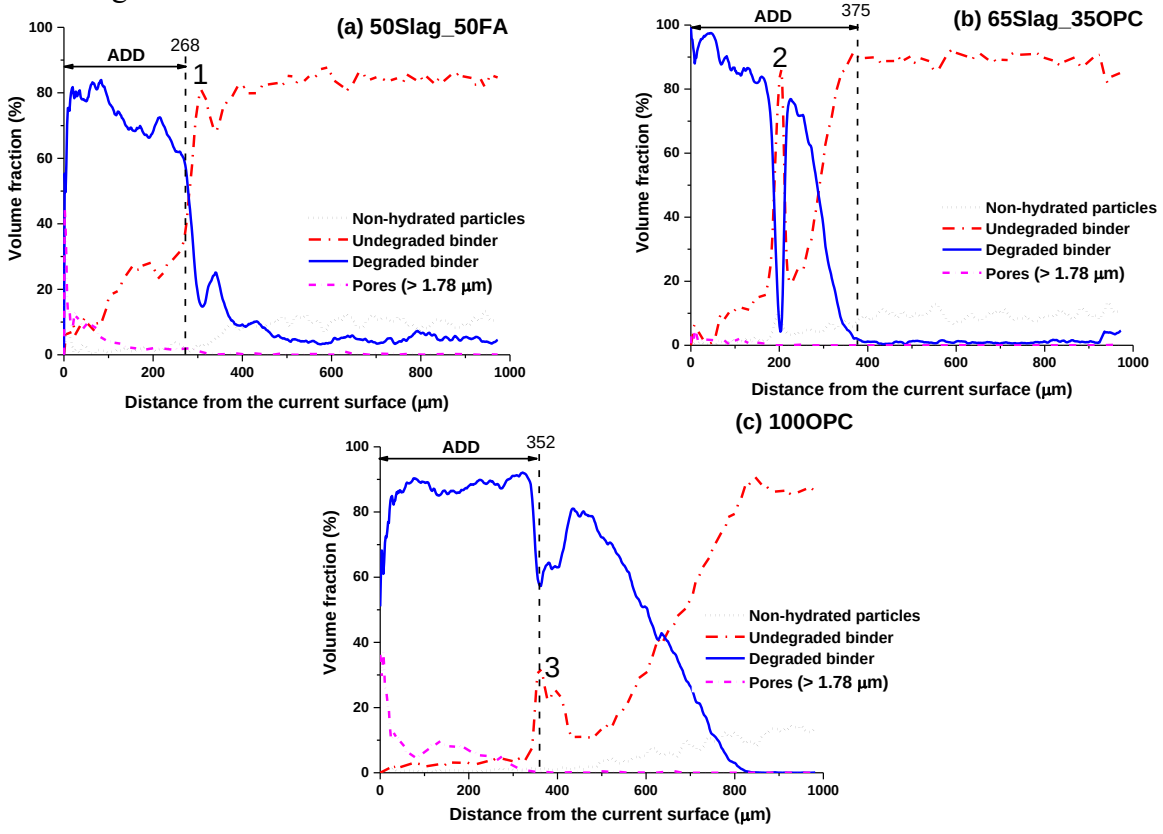


Fig. 12. Volume fractions of different components in three mixes after 21 days of immersion for (a) 50Slag_50FA, (b) 65Slag_35OPC and (c) 100OPC obtained from the current surface of the sample derived from micro-CT analysis. The ADD values are obtained from Fig. 3.

3.4. Dissolution rate of powdered samples

The results of Dissolution Rate (DR) and Normalized Dissolution Rate (NDR) are listed in Table 5. It is found that 100OPC got the largest NDR (0.087 g/m^2) followed by 65Slag_35FA (0.046 g/m^2) and 50Slag_50FA (0.041 g/m^2). Based on the previous dissolved depth (DD) as shown in Fig. 3(b), NDR and DD are consistent with each other: compared to the much larger NDR and DD for 100OPC, the two values for 65Slag_35FA and 50Slag_50FA are close with each other. The only difference is the immersion condition, one is powdered samples exposed to nitric acid and another one is cylindrical bulk samples immersed in the phosphoric acid. Therefore, the consistent results imply that both NDR and DD can be used to reflect the intrinsic chemical resistance of different binders having no influence of the following two factors: one is porous media in bulk samples (e.g. tortuosity and connectivity) [108, 109] and another is precipitations of various salts that may further block the surface or inner pores of samples, leading to some changes in degradation processes [110]. Similar to DD, the NDR of different binders reflects the intrinsic stability of various binding gels which is also likely due to the different Al and Ca contents: a higher aluminum but lower calcium content leads to a lower NDR.

Table 5

Detailed information on the dissolution rate test (48 hours of immersion for different powder mixes in the nitric acid solution).

Sample ID	Averaged M_{before} (g)	Averaged M_{after} (g)	S (m^2/g)	DR	NDR (g/m^2)
50Slag_50FA	0.2002	0.0940	13.07	0.53	0.041
65Slag_35FA	0.1998	0.0058	20.90	0.97	0.046
100OPC	0.2000	0.0195	10.39	0.90	0.087

Note: M_{before}-the mass of the powdered sample before exposure, M_{after}-the mass of the powdered sample after exposure, S-BET surface area, DR-Dissolution rate, NDR-Normalized dissolution rate.

4. Conclusions

This study demonstrates the early-stage behaviour of a type of AASF and two types of OPC-based binders exposed to phosphoric acid (pH = 2) in terms of their degradation kinetics and

related microstructural and mineralogical changes. A higher degradation rate was observed in the OPC-based binders, especially the 100OPC specimens. The AASF binder with GGBFS/FA at 1:1 exhibited an 'induction stage' within about 7-day degradation depth evolution, which is attributed to its higher neutralisation capacity. Using the leaching data, the calcium content in the binder composition is the most sensitive component of the binder towards acid attack whereas other elements as Al and Si seem relatively stable or negligibly affected. Hence, alternative binders, as here AASF, with a higher content of Al and Si displayed stronger resistance against the phosphoric acid, compared to the 100OPC. The stable highly crosslinking C-(A)-S-H, in the AASF led to the formation of a thicker transition zone which is beneficial for resisting further acid migration and also provides a solid space for the precipitation of different salts such as Brushite. In comparison, 100OPC binder had almost no transition zone and the main components were already partially degraded even when the pH was still higher than 8.3 due to a much higher calcium content introduced by OPC in the binding matrix. The calcium is released at the expense of losing structural integrity, facilitating more ingress of hydronium ions.

65Slag_35OPC seemed to present an intermediate behaviour between 50Slag_50FA and 100OPC pastes: it had the largest ADD value due to its lowest neutralisation capacity, similar to that of the 100OPC. However, it displayed a transition zone because of a relatively lower Ca content and higher content of Al and Si, leading to a similar DD as that of the 50Slag_50FA binder. Thus, it can be considered as an acceptable alternative to pure OPC binders.

Considering the initial highest capillary sorptivity of 50Slag_50FA and highest water absorption as well as VPV of 65Slag_35OPC prior to the acid immersion, it is concluded that the chemistry and structure of the gel formed in each cement has significantly more influence than their microstructural properties in determining the early-stage degradation performance.

Acknowledgements

The authors deliver great thanks to Chinese Scholarship Council (CSC), the Geopolymer and Mineral Processing Group laboratory in the University of Melbourne for financial and infrastructure support. This study was also supported by Mrs Laura Jukes who provided great help during the experimental parts. Thank you for the ARC Research Hub for Nanoscience-based Construction Material Manufacturing (IH150100006) for financial support.

References

[1] T.A. Aiken, W. Sha, J. Kwasny, M.N. Soutsos, Resistance of geopolymer and Portland cement based systems to silage effluent attack, Cement and Concrete Research 92 (2017) 56-65.

[2] S. Pavía, E. Condren, Study of the durability of OPC versus GGBS concrete on exposure to silage effluent, Journal of materials in civil engineering 20(4) (2008) 313-320.

[3] M.G.D. Gutiérrez-Padilla, A. Bielefeldt, S. Ovtchinnikov, M. Hernandez, J. Silverstein, Biogenic sulfuric acid attack on different types of commercially produced concrete sewer pipes, Cement and Concrete Research 40(2) (2010) 293-301.

[4] A. Parande, P. Ramsamy, S. Ethirajan, C. Rao, N. Palanisamy, Deterioration of reinforced concrete in sewer environments, Proceedings of the Institution of Civil Engineers-Municipal Engineer, Thomas Telford Ltd, 2006, pp. 11-20.

[5] L. Zhang, P. De Schryver, B. De Gusseme, W. De Muynck, N. Boon, W. Verstraete, Chemical and biological technologies for hydrogen sulfide emission control in sewer systems: a review, Water research 42(1-2) (2008) 1-12.

[6] J. Ren, L. Zhang, R.S. Nicolas, Degradation of Alkali-Activated Slag and Fly Ash Mortars under Different Aggressive Acid Conditions, Journal of Materials in Civil Engineering 33(7) (2021).

[7] K. Scrivener, N. De Belie, Bacteriogenic sulfuric acid attack of cementitious materials in sewage systems, Performance of cement-based materials in aggressive aqueous environments, Springer2013, pp. 305-318.

[8] J. Ren, L. Zhang, R. San Nicolas, Degradation process of alkali-activated slag/fly ash and Portland cement-based pastes exposed to phosphoric acid, Construction and Building Materials 232 (2020) 117209.

[9] Y. Xie, X. Lin, T. Ji, Y. Liang, W.J.C. Pan, B. Materials, Comparison of corrosion resistance mechanism between ordinary Portland concrete and alkali-activated concrete subjected to biogenic sulfuric acid attack, 228 (2019) 117071.

[10] H.B. Chang, Y.C.J.J.o.M.R. Choi, Technology, Accelerated performance evaluation of repair mortars for concrete sewer pipes subjected to sulfuric acid attack, 9(6) (2020) 13635-13645.

[11] A. Özcan, M.B.J.I.J.o.C.E. Karakoç, The resistance of blast furnace slag-and ferrochrome slag-based geopolymer concrete against acid attack, 17(10) (2019) 1571-1583.

[12] M. Vafaei, A. Allahverdi, P. Dong, N.J.C. Bassim, B. Materials, Acid attack on geopolymer cement mortar based on waste-glass powder and calcium aluminate cement at mild concentration, 193 (2018) 363-372.

[13] P. Sturm, G. Gluth, C. Jäger, H. Brouwers, H.-C.J.C. Kühne, C. Research, Sulfuric acid resistance of one-part alkali-activated mortars, 109 (2018) 54-63.

[14] H.A. Khan, A. Castel, M.S. Khan, A.H.J.C. Mahmood, C. research, Durability of calcium aluminate and sulphate resistant Portland cement based mortars in aggressive sewer environment and sulphuric acid, 124 (2019) 105852.

[15] A. Bertron, J. Duchesne, G. Escadeillas, Degradation of cement pastes by organic acids, Materials and structures 40(3) (2007) 341-354.

[16] S. Larreur-Cayol, A. Bertron, G. Escadeillas, Degradation of cement-based materials by various organic acids in agro-industrial waste-waters, Cement and Concrete Research 41(8) (2011) 882-892.

[17] O. Oueslati, J. Duchesne, The effect of SCMs and curing time on resistance of mortars subjected to organic acids, Cement and Concrete Research 42(1) (2012) 205-214.

[18] M. Alexander, C. Fourie, Performance of sewer pipe concrete mixtures with portland and calcium aluminate cements subject to mineral and biogenic acid attack, Materials and structures 44(1) (2011) 313-330.

[19] T. Gutberlet, H. Hilbig, R.E. Beddoe, Acid attack on hydrated cement — Effect of mineral acids on the degradation process, Cement and Concrete Research 74 (2015) 35-43.

[20] E. Galanos, K. Gray, A. Biddlestone, K. Thayanithy, The aerobic treatment of silage effluent: effluent characterization and fermentation, Journal of agricultural engineering research 62(4) (1995) 271-279.

[21] M.M. Gebrehanna, R.J. Gordon, A. Madani, A.C. VanderZaag, J.D. Wood, Silage effluent management: A review, Journal of Environmental Management 143 (2014) 113-122.
[22] J. Ren, S. Guo, J. Su, T. Zhao, J. Chen, S. Zhang, A novel TiO_2/Epoxy resin composited geopolymer with great durability in wetting-drying and phosphoric acid solution, Journal of Cleaner Production 227 (2019) 849-860.
[23] M. Secco, G.I. Lampronti, M.-C. Schlegel, L. Maritan, F. Zorzi, Degradation processes of reinforced concretes by combined sulfate–phosphate attack, Cement and Concrete Research 68 (2015) 49-63.
[24] J. Ren, L. Zhang, R. San Nicolas, Degradation of alkali-activated slag/fly ash mortars under different aggressive acid conditions, Journal of materials in civil engineering (2020).
[25] H. Yuan, P. Dangla, P. Chatellier, T. Chaussadent, Degradation modelling of concrete submitted to sulfuric acid attack, Cement and Concrete Research 53 (2013) 267-277.
[26] R.E. Beddoe, H.W. Dorner, Modelling acid attack on concrete: Part I. The essential mechanisms, Cement and Concrete Research 35(12) (2005) 2333-2339.
[27] S.A. Bernal, E.D. Rodríguez, R. Mejía de Gutiérrez, J.L. Provis, Performance of alkali-activated slag mortars exposed to acids, Journal of Sustainable Cement-Based Materials 1(3) (2012) 138-151.
[28] R.R. Lloyd, J.L. Provis, J.S.J. van Deventer, Acid resistance of inorganic polymer binders. 1. Corrosion rate, Materials and Structures 45(1) (2012) 1-14.
[29] S. Zhang, A. Keulen, K. Arbi, G. Ye, Waste glass as partial mineral precursor in alkali-activated slag/fly ash system, Cement and Concrete Research 102 (2017) 29-40.
[30] T. Yang, H. Zhu, Z. Zhang, X. Gao, C. Zhang, Q. Wu, Effect of fly ash microsphere on the rheology and microstructure of alkali-activated fly ash/slag pastes, Cement and Concrete Research 109 (2018) 198-207.
[31] X. Gao, Q. Yu, H. Brouwers, Reaction kinetics, gel character and strength of ambient temperature cured alkali activated slag–fly ash blends, Construction and Building Materials 80 (2015) 105-115.
[32] K. Goretta, N. Chen, F. Gutierrez-Mora, J. Routbort, G. Lukey, J. Van Deventer, Solid-particle erosion of a geopolymer containing fly ash and blast-furnace slag, Wear 256(7-8) (2004) 714-719.
[33] A. Wardhono, D.W. Law, A. Strano, The strength of alkali-activated slag/fly ash mortar blends at ambient temperature, Procedia Engineering 125 (2015) 650-656.
[34] A.R. Brough, A. Atkinson, Sodium silicate-based, alkali-activated slag mortars: Part I. Strength, hydration and microstructure, Cement and Concrete Research 32(6) (2002) 865-879.
[35] T.A. Aiken, J. Kwasny, W. Sha, M.N. Soutsos, Effect of slag content and activator dosage on the resistance of fly ash geopolymer binders to sulfuric acid attack, Cement and Concrete Research 111 (2018) 23-40.
[36] A. Bertron, G. Escadeillas, J. Duchesne, Cement pastes alteration by liquid manure organic acids: chemical and mineralogical characterization, Cement and Concrete Research 34(10) (2004) 1823-1835.
[37] F. Puertas, S. Martínez-Ramírez, S. Alonso, T. Vazquez, Alkali-activated fly ash/slag cements: strength behaviour and hydration products, Cement and concrete research 30(10) (2000) 1625-1632.
[38] F. Puertas, A. Fernández-Jiménez, Mineralogical and microstructural characterisation of alkali-activated fly ash/slag pastes, Cement and Concrete composites 25(3) (2003) 287-292.
[39] I. Ismail, S.A. Bernal, J.L. Provis, R. San Nicolas, S. Hamdan, J.S.J. van Deventer, Modification of phase evolution in alkali-activated blast furnace slag by the incorporation of fly ash, Cement and Concrete Composites 45 (2014) 125-135.
[40] A. Adam, Strength and durability properties of alkali activated slag and fly ash-based geopolymer concrete, School of Civil, Environmental and Chemical Engineering, RMIT University, 2009.
[41] N. Lee, H. Lee, Influence of the slag content on the chloride and sulfuric acid resistances of alkali-activated fly ash/slag paste, Cement and Concrete Composites 72 (2016) 168-179.
[42] W. Zhang, X. Yao, T. Yang, Z. Zhang, The degradation mechanisms of alkali-activated fly ash/slag blend cements exposed to sulphuric acid, Construction and Building Materials 186 (2018) 1177-1187.
[43] D.M. Roy, W. Jiang, M.R. Silsbee, Chloride diffusion in ordinary, blended, and alkali-activated cement pastes and its relation to other properties, Cement and Concrete Research 30(12) (2000) 1879-1884.

[44] I. Ismail, S.A. Bernal, J.L. Provis, S. Hamdan, J.S. van Deventer, Drying-induced changes in the structure of alkali-activated pastes, Journal of Materials Science 48(9) (2013) 3566-3577.
[45] ASTM C642, Standard test method for density, absorption, and voids in hardened concrete, ASTM International, 100 Barr Harbor Drive, PO Box C700, West Conshohocken, PA 19428–2959, United States, 2008.
[46] C. ASTM, 1585-04. Standard test method for measurement of rate of absorption of water by hydraulic-cement concretes, ASTM International (2004).
[47] A. ASTM, C109/C109M-Standard Test Method for Compressive Strength of Hydraulic Cement Mortars (Using 2-in. or (50-mm) Cube Specimens); 2013. 2, Scope of work shall include but not be limited to the following:-Suspended metal grid for acoustical tile ceiling system (1999).
[48] T. Bakharev, Resistance of geopolymer materials to acid attack, Cement and Concrete Research 35(4) (2005) 658-670.
[49] L.T. Angenent, K. Karim, M.H. Al-Dahhan, B.A. Wrenn, R. Domíguez-Espinosa, Production of bioenergy and biochemicals from industrial and agricultural wastewater, TRENDS in Biotechnology 22(9) (2004) 477-485.
[50] S. Wallah, B.V. Rangan, Low-calcium fly ash-based geopolymer concrete: Long-term properties, Curtin University of Technology, 2006.
[51] Y. Zuo, M. Nedeljković, G. Ye, Pore solution composition of alkali-activated slag/fly ash pastes, Cement and Concrete Research 115 (2019) 230-250.
[52] B. Huber, H. Hilbig, M.M. Mago, J.E. Drewes, E. Müller, Comparative analysis of biogenic and chemical sulfuric acid attack on hardened cement paste using laser ablation-ICP-MS, Cement and Concrete Research 87 (2016) 14-21.
[53] C. Magniont, M. Coutand, A. Bertron, X. Cameleyre, C. Lafforgue, S. Beaufort, G. Escadeillas, A new test method to assess the bacterial deterioration of cementitious materials, Cement and Concrete Research 41(4) (2011) 429-438.
[54] A. Bertron, J. Duchesne, G. Escadeillas, Attack of cement pastes exposed to organic acids in manure, Cement and Concrete Composites 27(9-10) (2005) 898-909.
[55] M. Hossain, M. Karim, M. Hasan, M. Hossain, M.F.M. Zain, Durability of mortar and concrete made up of pozzolans as a partial replacement of cement: A review, Construction and Building Materials 116 (2016) 128-140.
[56] L. Pel, K. Kopinga, E.F. Kaasschieter, Saline absorption in calcium-silicate brick observed by NMR scanning, Journal of Physics D: Applied Physics 33(11) (2000) 1380.
[57] M. Fournier, M. Odorico, E. Nicoleau, A. Ull, P. Frugier, S. Gin, Reactive Surface of Glass Particles Under Aqueous Corrosion, Procedia Earth and Planetary Science 17 (2017) 257-260.
[58] S.S. International Organization for Standardization. Technical Committee ISO/TC 24. Particle characterization including sieving, Particle characterization, Determination of the Specific Surface Area of Solids by Gas Adsorption: BET Method, ISO2010.
[59] E.C. Arvaniti, M.C. Juenger, S.A. Bernal, J. Duchesne, L. Courard, S. Leroy, J.L. Provis, A. Klemm, N. De Belie, Determination of particle size, surface area, and shape of supplementary cementitious materials by different techniques, Materials and Structures 48(11) (2015) 3687-3701.
[60] J.L. Bell, P.E. Driemeyer, W.M. Kriven, Formation of ceramics from metakaolin ‐ based geopolymers. Part II: K ‐ based geopolymer, Journal of the American Ceramic Society 92(3) (2009) 607-615.
[61] D.K. Panesar, J. Francis, Influence of limestone and slag on the pore structure of cement paste based on mercury intrusion porosimetry and water vapour sorption measurements, Construction and Building Materials 52 (2014) 52-58.
[62] A. Koenig, A. Herrmann, S. Overmann, F. Dehn, Resistance of alkali-activated binders to organic acid attack: Assessment of evaluation criteria and damage mechanisms, Construction and Building Materials 151 (2017) 405-413.
[63] J.J. Beaudoin, V. Ramachandran, A new perspective on the hydration characteristics of cement phases, Cement and Concrete research 22(4) (1992) 689-694.

[64] H.M. Jennings, Refinements to colloid model of CSH in cement: CM-II, Cement and Concrete Research 38(3) (2008) 275-289.
[65] A.J. Allen, J.J. Thomas, H.M. Jennings, Composition and density of nanoscale calcium–silicate–hydrate in cement, Nature materials 6(4) (2007) 311.
[66] C. Varga, M. Alonso, R.M. De Gutierrez, J. Mejía, F. Puertas, Decalcification of alkali-activated slag pastes. Effect of the chemical composition of the slag, Materials and Structures 48(3) (2015) 541-555.
[67] N. Ukrainczyk, O. Vogt, E.A. Koenders, Reactive transport numerical model for durability of geopolymer materials, Adv. Chem. Eng. Sci. 6(04) (2016) 355.
[68] P. Rajan, S. Rajendran, J. Sathiyabama, J.L. Christy, J. Jeyasundari, P. Prabhakar, Corrosion inhibitors for concrete corrosion-An Overview, European Chemical Bulletin 2(1) (2012) 1-8.
[69] R. Vera, M. Villarroel, A. Carvajal, E. Vera, C. Ortiz, Corrosion products of reinforcement in concrete in marine and industrial environments, Materials Chemistry and Physics 114(1) (2009) 467-474.
[70] M. Kouřil, P. Novák, M. Bojko, Threshold chloride concentration for stainless steels activation in concrete pore solutions, Cement and Concrete Research 40(3) (2010) 431-436.
[71] P. Feng, C. Miao, J.W. Bullard, A model of phase stability, microstructure and properties during leaching of portland cement binders, Cement and Concrete Composites 49 (2014) 9-19.
[72] A. Mehta, R. Siddique, Sulfuric acid resistance of fly ash based geopolymer concrete, Construction and Building Materials 146 (2017) 136-143.
[73] S. Thokchom, Fly ash geopolymer pastes in sulphuric acid, Int. J. Eng. Innovation Res 3(6) (2014) 943-947.
[74] O. Oueslati, J. Duchesne, Resistance of blended cement pastes subjected to organic acids: Quantification of anhydrous and hydrated phases, Cement and Concrete Composites 45 (2014) 89-101.
[75] N.M. Ukrainczyk, M.; Vogt, O.; Koenders, E, Geopolymer, Calcium Aluminate, and Portland Cement-Based Mortars: Comparing Degradation Using Acetic Acid, materials 12 (2019) 3115.
[76] Li, Zihui, Peethamparan, Sulapha, Leaching resistance of alkali-activated slag and fly ash mortars exposed to organic acid.
[77] A. Fernández‐Jiménez, F. Puertas, I. Sobrados, J. Sanz, Structure of calcium silicate hydrates formed in alkaline‐activated slag: influence of the type of alkaline activator, Journal of the American Ceramic Society 86(8) (2003) 1389-1394.
[78] S.-D. Wang, K.L. Scrivener, Hydration products of alkali activated slag cement, Cement and Concrete Research 25(3) (1995) 561-571.
[79] M.B. Haha, G. Le Saout, F. Winnefeld, B. Lothenbach, Influence of activator type on hydration kinetics, hydrate assemblage and microstructural development of alkali activated blast-furnace slags, Cement and Concrete Research 41(3) (2011) 301-310.
[80] C.R. Shearer, J.L. Provis, S.A. Bernal, K.E. Kurtis, Alkali-activation potential of biomass-coal co-fired fly ash, Cement and Concrete Composites 73 (2016) 62-74.
[81] L. Alarcon-Ruiz, G. Platret, E. Massieu, A. Ehrlacher, The use of thermal analysis in assessing the effect of temperature on a cement paste, Cement and Concrete research 35(3) (2005) 609-613.
[82] A. Fernández‐Jiménez, A. Palomo, J.Y. Pastor, A. Martin, New cementitious materials based on alkali‐activated fly ash: performance at high temperatures, Journal of the American Ceramic Society 91(10) (2008) 3308-3314.
[83] H. El Didamony, H.H. Assal, T.M. El Sokkary, H.A. Abdel Gawwad, Kinetics and physico-chemical properties of alkali activated blast-furnace slag/basalt pastes, HBRC Journal 8(3) (2012) 170-176.
[84] H.F. Taylor, Cement chemistry, Thomas Telford1997.
[85] M.A. Salih, N. Farzadnia, A.A. Abang Ali, R. Demirboga, Development of high strength alkali activated binder using palm oil fuel ash and GGBS at ambient temperature, Construction and Building Materials 93 (2015) 289-300.

[86] M. Thiery, G. Villain, P. Dangla, G. Platret, Investigation of the carbonation front shape on cementitious materials: effects of the chemical kinetics, Cement and Concrete Research 37(7) (2007) 1047-1058.
[87] N.Y. Mostafa, S.A.S. El-Hemaly, E.I. Al-Wakeel, S.A. El-Korashy, P.W. Brown, Characterization and evaluation of the hydraulic activity of water-cooled slag and air-cooled slag, Cement and Concrete Research 31(6) (2001) 899-904.
[88] C. Ruiz-Santaquiteria, J. Skibsted, A. Fernández-Jiménez, A. Palomo, Alkaline solution/binder ratio as a determining factor in the alkaline activation of aluminosilicates, Cement and Concrete Research 42(9) (2012) 1242-1251.
[89] F. Puertas, M. Palacios, A. Gil-Maroto, T. Vázquez, Alkali-aggregate behaviour of alkali-activated slag mortars: Effect of aggregate type, Cement and Concrete Composites 31(5) (2009) 277-284.
[90] J.A. Gadsden, Infrared spectra of minerals and related inorganic compounds, Butterworths1975.
[91] M.B. Haha, B. Lothenbach, G. Le Saout, F. Winnefeld, Influence of slag chemistry on the hydration of alkali-activated blast-furnace slag—Part II: Effect of Al2O3, Cement and Concrete Research 42(1) (2012) 74-83.
[92] M. Ben Haha, G. Le Saout, F. Winnefeld, B. Lothenbach, Influence of activator type on hydration kinetics, hydrate assemblage and microstructural development of alkali activated blast-furnace slags, Cement and Concrete Research 41(3) (2011) 301-310.
[93] R.L. Frost, S.J. Palmer, Thermal stability of the 'cave'mineral brushite CaHPO4· 2H2O–Mechanism of formation and decomposition, Thermochimica acta 521(1-2) (2011) 14-17.
[94] Q. Zhou, F.P. Glasser, Thermal stability and decomposition mechanisms of ettringite at< 120 C, Cement and Concrete Research 31(9) (2001) 1333-1339.
[95] A. Chaipanich, T. Nochaiya, Thermal analysis and microstructure of Portland cement-fly ash-silica fume pastes, Journal of Thermal Analysis and Calorimetry 99(2) (2009) 487-493.
[96] A.W. Decho, Overview of biopolymer-induced mineralization: What goes on in biofilms?, Ecological Engineering 36(2) (2010) 137-144.
[97] B. Lothenbach, G. Le Saout, E. Gallucci, K. Scrivener, Influence of limestone on the hydration of Portland cements, Cement and Concrete Research 38(6) (2008) 848-860.
[98] M. Zajac, A. Rossberg, G. Le Saout, B. Lothenbach, Influence of limestone and anhydrite on the hydration of Portland cements, Cement and Concrete Composites 46 (2014) 99-108.
[99] B. Dilnesa, B. Lothenbach, G. Le Saout, G. Renaudin, A. Mesbah, Y. Filinchuk, A. Wichser, E. Wieland, Iron in carbonate containing AFm phases, Cement and Concrete Research 41(3) (2011) 311-323.
[100] T. Nochaiya, W. Wongkeo, K. Pimraksa, A. Chaipanich, Microstructural, physical, and thermal analyses of Portland cement–fly ash–calcium hydroxide blended pastes, Journal of thermal analysis and calorimetry 100(1) (2009) 101-108.
[101] N. Marjanović, M. Komljenović, Z. Baščarević, V. Nikolić, R. Petrović, Physical–mechanical and microstructural properties of alkali-activated fly ash–blast furnace slag blends, Ceramics International 41(1, Part B) (2015) 1421-1435.
[102] A. Bertron, J. Duchesne, G. Escadeillas, Accelerated tests of hardened cement pastes alteration by organic acids: analysis of the pH effect, Cement and Concrete Research 35(1) (2005) 155-166.
[103] J. Temuujin, A. Minjigmaa, M. Lee, N. Chen-Tan, A. van Riessen, Characterisation of class F fly ash geopolymer pastes immersed in acid and alkaline solutions, Cement and Concrete Composites 33(10) (2011) 1086-1091.
[104] N. Lee, H. Lee, Reactivity and reaction products of alkali-activated, fly ash/slag paste, Construction and Building Materials 81 (2015) 303-312.
[105] S.M. Park, J.G. Jang, N. Lee, H.-K. Lee, Physicochemical properties of binder gel in alkali-activated fly ash/slag exposed to high temperatures, Cement and Concrete Research 89 (2016) 72-79.
[106] S.A. Bernal, J.L. Provis, B. Walkley, R. San Nicolas, J.D. Gehman, D.G. Brice, A.R. Kilcullen, P. Duxson, J.S.J. van Deventer, Gel nanostructure in alkali-activated binders based on slag and fly ash, and effects of accelerated carbonation, Cement and Concrete Research 53 (2013) 127-144.

[107] M. Königsberger, J. Carette, Validated hydration model for slag-blended cement based on calorimetry measurements, Cement and Concrete Research 128 (2020) 105950.
[108] B. Johannesson, Nonlinear transient phenomena in porous media with special regard to concrete and durability, Advanced Cement Based Materials 6(3-4) (1997) 71-75.
[109] J.S. Van Deventer, J.L. Provis, P. Duxson, Technical and commercial progress in the adoption of geopolymer cement, Minerals Engineering 29 (2012) 89-104.
[110] L. De Windt, P. Devillers, Modeling the degradation of Portland cement pastes by biogenic organic acids, Cement and Concrete Research 40(8) (2010) 1165-1174.